Aus dem der Medizinischen Klinik m. S. Kardiologie und Angiologie
der Medizinischen Fakultät Charité – Universitätsmedizin Berlin

DISSERTATION

Ultrastructural and Compositional Changes in Heart Muscle Cells in Mouse Model of Viral Myocarditis as Imaged by Infra-red Spectromicroscopy

zur Erlangung des akademischen Grades
Doctor medicinae (Dr. med.)

vorgelegt der Medizinischen Fakultät
Charité – Universitätsmedizin Berlin

von

Wasiem G.E. Sanad
aus Kairo, Ägypten

Gutachter: 1. Priv.-Doz. Dr. med. Th. Dschietzig

2. Priv.-Doz. Dr. med. D. Kivelitz

3. Prof. Dr. med. A. May

Datum der Promotion: 21. November 2008

Contents

I. Introduction

Myocarditis is a non-ischemic inflammatory process involving the heart muscle cells (myocytes) with variable clinical outcomes. In most cases the disease is self limiting; however, it may lead to acute heart failure, resulting in early death or heart transplantation[1]. Postmortem data have implicated myocarditis in sudden cardiac death of young adults at rates of 8.6% to 12%[2].

Although bacteria, fungi and parasites cause myocarditis, viral infection is most common[3]. Among the most commonly identified infectious viral agents are the Coxsackieviruses Bs, members of the enterovirus genus of the picornavirus family[4]. Reports of isolation of Coxsackievirus from the heart or pericardial fluid of patients with acute myocarditis date back as far as 1965[5]; with numerous reports since of the virus isolated from the cardiac tissue or pericardial fluid or showing the presence of viral antigens in diseased heart tissue[6].

In addition to the clear association between enteroviral infection and acute myocarditis, it has been shown that chronic, dilated cardiomyopathy can be a sequela of viral yocarditis[7]. And myocarditis has been identified as a cause of dilated cardiomyopathy in 9% of cases[8]

Dilated cardiomyopathy is characterized by increased left ventricular or biventricular dimensions with decreased left ventricular ejection fraction and is not caused by abnormal loading conditions or coronary ischemia. Myocardial contractility is severely impaired and labelled “systolic Failure”. Dilated cardiomyopathy is largely an irreversible form of heart muscle disease with an estimated prevalence of 1:2500; it is the third most common cause of heart failure and the most frequent cause of heart transplantation[9]. The annual incidence of dilated cardiomyopathy in Europe is 59,000 cases[10].

Attempts to isolate the virus from the myocardium in patients with dilated cardiomyopathy have so far been unrewarding. However, enteroviral RNA and antigen in myocardial tissue of patients with DCM has been achieved by serological and molecular biological

techniques such as slot-blot, in situ hybridization, and reverse transcription polymerase chain reaction.

Evaluation of some patients suspected of suffering from cardiomyopathy has been facilitated by the use of endomyocardial biopsy. However, the clinical utility of routine biopsy is limited, particularly because no definitive pattern has been found in dilated cardiomyopathy. A specific etiological diagnosis is obtained by biopsy in only about 10% of patients with cardiomyopathy[11], and a treatable disease is found even less often.

Newer techniques are therefore needed to further expand the diagnostic utility of endomyocardial biopsy in patients with myocarditis and cardiomyopathy.

II. Background

Understanding the chronic changes in heart function following myocarditis relies on detecting the compositional changes that occur in the cardiac myocytes, as well as those in the extracellular matrix.

In the heart, an intricate lattice of collagen-containing extracellular matrix (ECM) surrounds individual myocytes and myofibril bundles, ensuring correct tissue geometry and aiding efficient vectoral transmission of force. The extracellular matrix is a complex mixture of collagen fibrils, elastin, cells including fibroblasts[12] and macrophages, macromolecules such as glycoproteins, and glycosaminoglycans together with other molecules such as growth factors, cytokines, and extracellular proteases.

The concept that the extracellular matrix is inert has evidently been overturned. Excessive collagen, the main extracellular matrix protein, clearly is detrimental to cardiac function[13]. Collagen deposition can be controlled by hormones such as angiotensin II and aldosterone[14]. Chronic activation of the renin-angiotensin system is associated with the appearance of inflammatory cells and fibroblasts in the perivascular space preceding the changes to the vasculature that lead to perivascular fibrosis[15].

Maladaptive remodeling of the cardiac ECM is observed in various disease states[16] and may contribute to systolic dysfunction through alterations in the tensile properties of the myocardium and in myocyte orientation[17].

However, apparent contradictions exist regarding the collagen content of the myocardium in disease states. Whereas collagen loss and fragmentation in heart failure have been observed in some studies, myocardial fibrosis has been noted in others[18,19,20,21]. Fibrosis is then believed to increase ventricular stiffness and reduce compliance and further impair myocardial mechanical function.

Myocardium of susceptible CVB3-infected mice typically shows fibrosis, which is characterized by excess deposition of mainly collagen type I beyond 14 days post infection[22].

II.1. Available methods:

Traditional techniques used for the detection of changes in cardiac extracellular matrix include trichrome staining, Western blot analysis, immunohistochemistry, Northern analysis, tissue 4-hydroxyproline concentration, and scanning electron microscopy.

Of the techniques just mentioned, only immunohistochemistry and scanning electron microscopy are able to provide information concerning the in vivo spatial distribution of organ collagens[23].

III. Objectives of the current work

To the best of our knowledge, no study has used infra-red spectromicroscopy to detect the changes encountered in the myocardium of Coxsackievirus-induced myocarditis in mouse models.

The present study hypothesized that infra-red spectromicroscopy can detect potentially important changes in murine myocarditis. The primary purpose was to determine whether infection of the myocardium with Coxsackievirus B3 leads to spectroscopical changes detectable by infra-red spectromicroscopy and to detect the properties of the cardiac extracellular matrix change during the transition from viral myocarditis to overt cardiomyopathy.

Mice were infected with Coxsackievirus B3 (CVB3) and Fourier transform infrared imaging (FTIRI) was used to examine two Coxsackievirus B3-induced mouse models of myocarditis: C57BL/6 and ABY/SnJ, which have been shown in previous studies to reflect the acute and chronic forms of the disease, respectively. The protein (especially collagen) and lipid content of heart tissue were examined at various time points after infection in order to characterize the chemical differences as a function of immunocompetence.

IV. Myocarditis and inflammatory cardiomyopathy in humans

IV.1. Aetiologies of myocarditis

Acute or chronic inflammatory process affecting the myocardium (myocarditis) can be caused by a wide variety of toxins and drugs (e.g., cocaine, interleukin 2) or infectious agents, most commonly viral (e.g. coxsackievirus, adenovirus, parvovirus, HIV), bacterial (e.g., diphtheria, meningococcus, psittacosis, streptococcus), rickettsial (typhus, Rocky Mountain spotted fever), fungal (e.g., aspergillosis, candidiasis), as well as Wipple disease (intestinal lipodystrophy), giant cell myocarditis, and hypersensitivity reactions to drugs such as antibiotics, sulphonamides anticonvulsants, and antiinflammatories. Viral myocarditis in utero (mumps) causes endocardial fibroelastosis (dilated cardiomyopathy in infants and children[9]).

The RNA core coxsackievirus has been identified as the most frequent viral agent responsible for myocardial inflammation[24]. A causal relationship between symptomatic presentation and rising serum Coxsackie B viral titres has been suggested[25]. In addition, nested polymerase chain reaction (PCR) analyses of adult and paediatric myocardium have also demonstrated the presence of adenoviral genome in patients with idiopathic left ventricular dysfunction.

Age-related and regional differences seem to play a relevant role in the viral aetiology of myocarditis.
Hepatitis C has been identified more frequently in Japanese patients, whereas parvovirus B19 genome is more commonly identified in German patients[26,27]. Hepatitis C virus antibodies and RNA have been identified in sera and cardiac tissues in patients with biopsy-proven myocarditis[27,28,29].
Human immunodeficiency virus (HIV) is associated with cardiotrophic viral infection resulting in myocarditis. Histological myocarditis was detected in 52% of cases with advanced HIV disease and global left ventricular dysfunction[30] and in 67% of HIV infected cases in a post-mortem analysis[31]. HIV-related myocarditis has a significantly poor

prognosis and has been identified as the strongest predictor of death among a large cardiomyopathy population[32]. A prospective study of asymptomatic HIV-infected patients revealed a mean incidence of progression to dilated cardiomyopathy of 15.9% per 1000 patients[33], with the incidence being higher with CD4+ counts < 400 cells/mm^3. Evidence of myocarditis was detected in 83% of these high-risk patients. In situ hybridization identified HIV-related myocarditis in 76% of this population. Whether the virus itself, medications used for its treatment, or myocardial coinfection is responsible for the left ventricular impairment remains unclear.

Therefore, the contemporary molecular techniques have substantiated the perception that viral infection plays a dominant role in the development of active myocarditis. Viral myocarditis remains the prototype for the study of the disease and its evolution.

Coxsackievirus has been the most commonly identified viral agent implicated in acute and chronic myocarditis.

IV.2. Coxsackieviral myocarditis

Coxsackievirus is an enterovirus, a member of the picornavirus family. Enteroviruses constitute a major subgroup of small RNA viruses that readily infect the gastrointestinal tract epithelial and lymphoid tissue. They include the polioviruses, coxsackieviruses, echoviruses, and the more recently discovered agents that are simply designated enteroviruses. These are extremely small (22-30 nm in diameter), naked virions with eicosahydral symmetry. Enteroviruses possess single-stranded, positive-sense RNA and a capsid formed from 60 copies of non-glycosylated proteins (VP1, VP2, VP3, and VP4). Replication and assembly occur exclusively in the cellular cytoplasm; one infectious cycle can occur within 6 to 7 hours. This results in cessation of host cell protein synthesis and cell lysis with the release of new infectious progeny.

Enteroviruses are quite resistant to acid pH (as low as 3.0). This feature helps ensure their safe passage through the stomach to the intestines. They are resistant to many common

disinfectants such as 70% alcohol, substituted phenolics, and ether. Chemical agents, such as 0.3% formaldehyde or free residual chloride at 0.3 to 0.4%, are effective; however, if sufficient extraneous organic debris is present, the virus can be protected and survive over longer periods. Most enteroviruses can be isolated in primates (human or simian) cell cultures and show characteristic cytoplasmic effects.

Coxsackievirus A serotypes, in particular, are more readily detected by inoculation of newborn mice. In fact, the newborn mouse is one basis for originally classifying group A and B coxsackieviruses. Coxsackieviruses are widely distributed in the world. Humans are the main natural host. Direct or indirect faecal-oral transmission is considered the most common mode of spread. After infection, the virus persists in the oropharynx for 1 to 4 weeks, and can be shed in the faeces for 1 to 18 weeks. Incubation period varies, but relatively short intervals (2 to 10 days) are frequent.

Coxsackievirus group B (subgroup 2, 3, 4, 5) are the enteroviruses most commonly implicated in the acute inflammation of heart muscle (myocarditis) or its covering membranes (pericarditis). The consequences of infection with these agents are highly variable and related only in part to virus subgroup and serotype. Up to 60% of infections are subclinical.

IV.3. Pathogenesis

Derived largely from animal models, three essential pathways have been described[34].
Direct myocardial invasion by cardiotrophic virus or other infectious agents rapidly progresses to a second phase of immunologic activation. In the last phase, CD4+ activation prompts clonal expansion of B cells, resulting in further myocytolysis, additional local inflammation, and the production of anti-heart antibodies.
All three mechanisms may interact within the same host; the predominant pathologic mechanism may vary according to host defences[35].

Following entry through the respiratory or gastrointestinal tract, the virus soon replicates, escapes the port of entry immunological response and is transported to the blood stream causing a systemic viraemia on days 0 to 3. Cytokine release activates the cardiac immune process. Two receptors, the Coxsackie-adenovirus receptor (CAR) and decay-accelerating factor (DAF), have been identified that play an important role in the attachment of the virus to the cardiac cell and initiation of infectious cycle in the myocytes[36]. Once in the cell, the myocyte translational apparatus translates the viral RNA as a monocistronic polyprotein that is subsequently cleaved into the individual viral polyproteins by the viral proteases. Viral RNA is replicated through a negative-strand RNA intermediate that serves as a template for positive-strand replicates which are encapsidized into new virions. The acute infectious cycle is usually completed by myocytolysis. Viral genomic persistence via incorporated double-stranded DNA may also contribute to myocyte dysfunction by cleaving dystrophin or eukaryotic initiation of Factor-4. In the following few days (2 to 7 days) dendritic cells and macrophages within the myocyte ingest the viral agents and there is a generalised immune response associated with a histological inflammatory infiltrate, with the subsequent expression of proinflammatory cytokines, particularly interleukin-1, interleukin-6, TNF[37,29]. TNF activates endothelial cells, recruits additional inflammatory cells, and has direct negative inotropic effects[3].

Cytokines also activate inducible NO synthase (NOS) in cardiac myocytes. The role of NO in the development and progression of myocarditis is complex. NO can inhibit viral replication by targeting specific viral proteases, and peroxynitrate formation has potent antiviral effects. NOS-deficient mice have greater viral titres, a higher viral load, and more widespread myocyte necrosis[38]. On the other hand, in experimental myosin-induced autoimmune myocarditis, NOS expression in myocytes and macrophages is associated with more inflammation, whereas NOS inhibitors have been shown to reduce myocarditis severity[38].

Cell-mediated immunity also plays an important role in viral clearance. Cytotoxic (CD8+) cells recognize viral protein fragments that are presented by major histocompatibility-complex class I antigens on the myocyte surface[39]

Finally, circulating autoantibodies directed against contractile, structural, and mitochondrial proteins have been described in both murine and human myocarditis. One or more

autoantibodies have been observed in 25% to 73% of patients with biopsy-proven disease[28] These autoantibodies may have direct cytopathic effects on energy metabolism, calcium homeostasis, and signal transduction. They can also induce complement activation with lysis of antibody-coated cells[40]. Removal of circulating autoantibodies by immunoadsorption has been shown to improve cardiac function and decrease myocardial inflammation[41].
In the following week and beyond, there may be a transition to idiopathic dilated cardiomyopathy, the mechanism of which has been only partially clarified by molecular techniques. Detection of viral RNA at early, intermediate, and late stages of myocardial infection has been demonstrated in murine models of viral myocarditis[42].

The presence of low levels of ongoing viral replication may result in progressive myocardial damage, including apoptotic cell death, as a result of the immunologic response to infection[37]. Persistence of viral particles has also been demonstrated in patients with dilated cardiomyopathy[43,6]. When matched with an activated immune system, viral persistence, even without replication, has been shown to induce dilated cardiomyopathy[43]. Furthermore, cytokines have been shown to remain elevated beyond 80 days [128].

Ultimately, acute and chronic myocardial damage may lead to coronary microvascular spasm, resulting in myocyte necrosis, fibrosis, calcification and cardiac dilatation[44]. Endothelial cell dysfunction and distortion of nitric oxide production can contribute to microvascular spasm[44,45].

IV.4. Changes in extracellular matrix

The relevant role of fibrosis in the development of organ pathology is increasingly recognized. A number of different cardiac pathologies seem to be caused by a fibrotic process[46]. Within the heart, this fibrosis is thought to be partially mediated by transforming growth factor-α (GF-α), a potent profibrotic cytokine that stimulates the production of

extracellular matrix proteins (a potent stimulator of collagen-producing cardiac fibroblasts), as evidenced by overexpression and knockout models[47,48,49,50].
The increased presence of extracellular matrix proteins within the myocardium results in an alteration of ventricular properties that causes both systolic and diastolic dysfunction[51].
TGF-α -associated fibrosis also results in an inhomogeneous milieu for electrical propagation, leading to the development of arrhythmia[52]. Similarly, excessive production of extracellular proteins within the heart valves results in leaflet thickening and impaired motion with associated valvular dysfunction[53].

In patients with dilated cardiomyopathy, collagen type I and III, as well as the collagen type I/type III ratio, were all shown to be elevated[54].
Sanderson et al. noted that the plasma levels of TGF-α were twice as high in patients who had developed idiopathic dilated cardiomyopathy when compared to controls[55].
Levels of TGF-α were also increased in macrophages present within the myocardial tissue of the dilated heart. In addition, genetic studies have also hinted at the possible involvement of TGF-alpha in dilated cardiomyopathy[56,57].

IV.5. Clinicopathological events after infection with coxsackievirus in humans

Manifestations of myocarditis range from asymptomatic ECG abnormalities to cardiogenic shock[58]. Patients may report a viral prodrome of fever, myalgia, respiratory symptoms, or gastroenteritis followed by an abrupt onset of haemodynamic collapse[59]. The incidence of a reported infectious viral prodrome is highly variable and ranges from 10% to 80% of patients with documented myocarditis[60,3].
Acute dilated cardiomyopathy is the most dramatic and clinically relevant presentation of acute lymphocytic myocarditis[61].

The link between clinical myocarditis and acute dilated cardiomyopathy is most convincingly demonstrated by endomyocardial biopsy findings[58]. But neither symptoms nor clinical course of myocarditis has been shown to correlate with the histological features of lymphocytic infiltrates or fibrosis[61].

The classification by Liebeman et al. differentiated several forms of presentations[62]. These are fulminant, acute (subacute), chronic active, and chronic persistent myocarditis.

Fulminant myocarditis has a distinct viral prodrome, fever, and an abrupt onset of severe global left ventricular dysfunction manifested by profound haemodynamic compromise requiring high dose vasopressor support. There is minimal left ventricular dilatation, but rather thickened left ventricular walls (probably as a manifestation of interstitial oedema). The endomyocardial biopsy shows multiple foci of inflammatory infiltrate and necrosis. Of note, either borderline or active lymphocytic myocarditis can produce this dramatic clinical presentation[59]. Patients die within 2 weeks or recover with complete histological and functional recovery of the myocardium[63].

Patients with acute (subacute) myocarditis present with moderately severe ventricular dysfunction without evidence of preceding clinical viral illness. The left ventricle is mildly dilated. The endomyocardial biopsy shows active or borderline myocarditis. Patients undergo complete recovery with complete resolution of histological inflammation, or progress to dilated cardiomyopathy with viral persistence. Recovered patients have the same relatively poor prognosis as those with dilated cardiomyopathy[45].

The onset of chronic active myocarditis is indistinct with moderate ventricular dysfunction. The endomyocardial biopsies at presentation and in follow-up reveal a combination of active myocarditis and active healing. These patients display ongoing inflammation and fibrosis resulting in the development of a restrictive (non-dilated) cardiomyopathy usually 2 to 4 years after presentation[62].

Patients with chronic persistent myocarditis manifest with non-heart failure-related symptoms (atypical chest pain or palpitations), because of which they are submitted to endomyocardial biopsy. They have normal left ventricular function despite having active or borderline myocarditis on biopsy.

Myocarditis can also be masquerading as an acute coronary syndrome[64,65]. Elevated troponin levels have proven to be a more reliable predictor of myocardial damage than levels of CK[66].

Electrocardiographically, there are changes suggestive of myocardial ischemia[66]. Despite angiographically normal coronary anatomy, echocardiography frequently shows evidence of segmental or global wall motion abnormalities[64]. Using myocardial indium[111]-labeled antimyosin antibody and rest thallium imaging, Sarda et al. identified 35 of 45 patients (78%) who presented with symptoms and signs consistent with acute coronary syndrome as having myocarditis (biopsy verification was not undertaken in this series)[65]. In another study of 34 patients presenting with symptoms and signs consistent with acute coronary syndrome, 11 patients (32%) were found to have myocarditis on biopsy[67]. Myocarditis masquerading as myocardial infarction almost universally results in a full recovery of cardiovascular status in previously healthy adults[59,64,67,65].

In sum, the disparity between the pathological findings of myocarditis and the clinical manifestations is well recognized. Furthermore, clinical practice guidelines are lacking despite the well established morbidity and mortality association with the disease[63,61,60].

IV.6. Investigative Evaluation of Myocarditis

Thus far, evaluation of myocarditis includes biopsy-based and non-biopsy-based methods.

IV.6.1. Biopsy-based methods

IV.6.1.1. Endomyocardial biopsy

Sakakibara and Konno described transvenous endomyocardial biopsy in the early 1960s[121]. Over years, the equipment and technique have evolved to the point where satisfactory tissue samples can be easily obtained in over 90% of diagnostic attempts and even more often in transplanted hearts[68].

Using a flexible bioptome, samples from the right ventricle (and from the left ventricle when required) may be obtained, usually under fluoroscopic guidance, through a transvenous (or transarterial) approach[72].

The right internal jugular vein is the most common percutaneous access for the right ventricular endomyocardial biopsy in the United States. In Germany and Italy, the femoral vein is commonly used[69]. The subclavian vein may also be used occasionally. The femoral artery may be used as a percutaneous access for left ventricular biopsy[70].

No comparative studies exist for left versus right ventricular biopsy; however, left ventricular biopsy has been used in case series to define cardiomyopathic processes limited to the left ventricle[71].

Ideally, samples should be obtained from more than one region of the right ventricular septum, and sample size should be 1 to 2 mm^3. Clinical considerations determine how many biopsy samples are to be obtained and how they are to be fixed. Usually four to five samples are obtained and transferred to a fixative at room temperature (10% neutral buffered formalin). One or more samples may be frozen for further studies.

IV.6.1.1.a. Histopathology

The adoption of Dallas criteria has helped improve the interpretation of finding[11]. However, there remains a lack of agreement about the diagnostic usefulness of any proposed scheme that utilizes conventional histological findings to evaluate inflammatory cardiomyopathy[73,74].

However, despite the evident progress in the design and techniques, shortcomings of the utility of endomyocardial biopsy still exist; including: (1) small sample size, (2) heterogeneous distribution of tissue pathology in many cardiac diseases leading to inherent sample errors, (3) subjective pathological interpretation of the microscopic findings (a high degree of interobserver variability), and (4) unknown true-positive/false-positive and true-negative/false-negative rates for biopsy finings in most diseases[75].

A considerable sampling error is associated with the interpretation of endomyocardial biopsy findings. Chow et al. and Hauck et al. have demonstrated by biopsying postmortem hearts of patients who had died from myocarditis that, from a single endomyocardial biopsy, histological myocarditis could be demonstrated in only 25% of samples. With more than five samples, Dallas criteria could be diagnosed in approximately two thirds of subjects[76,77]. A recent MRI study using focal imaging abnormalities to guide endomyocardial biopsy demonstrated that the earliest myocardial inflammatory abnormalities were evident in the lateral wall of the left ventricle and that only these sites revealed myocarditis by histological examination[71].

The high degree of interobsever variability was shown by the Myocarditis Treatment Trial. Of the 111 patients diagnosed with endomyocardial biopsy, only 64% had that diagnosis confirmed by the expert pathology panel who reviewed the histopathological material[60].

In addition, viral material can exist in the myocardium (even in a replicative form) in patients with viral myocarditis in the absence of myocardial inflammation adequate to meet the Dallas criteria and may adversely affect the outcome[78]. In a study by Martin et al. it was demonstrated in 34 children with clinical presentations compatible with myocarditis that 26 heart biopsy samples were positive for viral pathogens, and 13 of the 26 positive samples had no evidence of myocarditis on histopathological examination[79].

Another drawback of conventional histopathological findings is the dissociation between them and response to immune modulation therapy. In the Myocarditis Treatment Trial, there was no difference in the 1- or 5-year survival or 28-week ejection fraction in patients with Dallas criteria myocarditis treated with immunosuppressive therapy or placebo[60].

Taken together, the current histopathological criteria (Dallas criteria) are not sensitive enough to identify the population with viral or autoimmune-related heart compromise. Despite complete evaluation, including history, clinical examination, blood work, echocardiography, coronary angiography, and endomyocardial biopsy, no aetiology was identified in about 50% of patients with dilated cardiomyopathy[8].

IV.6.1.1.b. Immunological tools

Immunohistochemistry staining of samples obtained by endomyocardial biopsy enables more precise characterization of infiltrating lymphocyte subtypes[80]. It also helps define and quantify upregulation of major histocompatibility (MHC) antigens. Myocyte-specific MHC expression approach is said to have greater sensitivity than the Dallas criteria[81].

In a small study cohort by Herskowitz et al., the sensitivity and specificity of any MHC expression for detecting biopsy-proven myocarditis were 80% and 85%, respectively[30]. Surprisingly, a more recent larger cohort study of 83 patients with suspected myocarditis[82] found no correlation between MHC immunostaining and histopathological findings of active myocarditis by Dallas criteria. The study investigators argue that MHC expression could represent a chronic form of myocardial injury and may not be responsible for the patients' clinical presentation. This discordance is currently unexplained because the staining methods and patient population appeared to be similar[59].

Despite this discordance, assessment of MHC expression has recently been used to guide therapy of patients with inflammatory cardiomyopathy[83].

IV.6.2. Non-biopsy-based methods:

IV.6.2.1. Cardiac and other biomarkers:

Serum biomarkers (creatine kinase [CK], troponin I and T) are routinely measured when myocarditis is suspected. CK or its isoform (CK-MB) is not generally useful for screening because of its low predictive value. Elevated troponin levels have proven to be a more reliable predictor of myocardial damage than creatine kinase levels[66].

The erythrocyte sedimentation rate was shown in an early trial to have a very low sensitivity and specificity[84].

Other serum biomarkers such as complement, cytokines, and anti-heart antibodies, have not been prospectively validated to accurately screen for biopsy-proven myocarditis[85].

IV.6.2.2. Noninvasive imaging modalities

IV.6.2.2. a. **Echocardiography:**

Transthoracic echocardiography is routinely performed in the initial work-up of all patients with suspected myocarditis, with findings that can be varied and relatively nonspecific. Although anatomic features (i.e. chamber dimensions, ejection fraction, wall motion abnormalities) can differentiate myocarditis from other forms of cardiomyopathy, ultrasound tissue characterization, tissue Doppler, and myocardial velocity measurements may better characterize tissue changes in acute myocarditis and monitor changes over time[59].

IV.6.2.2. b. **Indium^{111}-labeled monoclonal antibody fragments**

Antimyosin cardiac uptake reflects the extent of myocardial necrosis. Indium^{111}-labeled monoclonal antibody fragments (directed against heavy chain myosin) bind to the cardiac myocytes that have lost the integrity of their sarcolemmal membranes and have exposed their intracellular myosin to the extracellular space. On the basis of endomyocardial biopsy, antimyosin uptake was found by Dec et al. to be highly sensitive (83%) but only moderately specific (53%) for detecting myocardial necrosis[86].
It has been reported that a positive antimyosin scan and a nondilated left ventricular cavity (left ventricular end-diastolic dimension <62 mm) was highly predictive for detecting myocarditis on biopsy[87].

IV.6.2.2. c. **Galium^{67}-labeled cardiac scintigraphy**

This modality detects the extent of myocardial inflammation. A sensitivity of 6% and a specificity of 98% for histological detection of myocarditis were reported[88].

IV.6.2.2. d. **Contrast-enhanced magnetic resonance imaging (MRI)**

In addition to anatomic and morphological information, MRI can provide accurate tissue characterization by measuring T1 and T2 relaxation times and spin densities. Assessment of relaxation times provides a sensitive measure for myocyte injury, including oedema and cellular swelling[89]. New contrast MR techniques using segmental inversion recovery gradient-echo pulse sequences and both early and late gadolinium enhancement provide substantial improvement in contrast between diseased and normal myocardium[90].

V. Experimental models of enteroviral cardiomyopathy

Although enteroviruses such as Coxsackie B viruses have been strongly associated with the pathogenesis of myocarditis and the evolution of dilated cardiomyopathy, the limitations of the current diagnostic strategies and clinical therapies make it difficult to understand the mechanisms by which enteroviral infection causes cardiomyopathy. Fortunately, there are well characterized murine models of CVB infection that provide a framework for studying the general pathogenic mechanisms.

V.1. Murine model of acute coxsackieviral myocarditis:

Virus-mediated myocytotoxicity has been demonstrated in vivo in acute viral infection. Coxsackievirus infection can induce a direct cytopathic effect in cultured foetal human[91], murine[92] and rat heart cells[43]. The direct virus-induced cytotoxicity includes the presence of necrotic myofibrils in the absence of an inflammatory cell infiltrate 3 days post infection[93], extensive cardiac damage in severe combined immunodeficiency and athymic mice, where the unusual inflammatory cell infiltrate is genetically reduced or absent[94], and lack of benefit of immunosuppressive therapy in several strains of inbred mice[95].

V.2. Murine model of chronic dilated cardiomyopathy caused by Coxsackievirus infection:

It has been shown that experimental viral myocarditis could be associated with persistence of inflammation progressing to myocardial fibrosis. Wilson et al. found that acute infection with Coxsackievirus B3 in Swiss mice was followed by marked fibrosis, dystrophic mineralization, and microscopic myocardial hypertrophy, which persisted for at least 6 months[96]. Cardiomyopathy evolved in the infected mice in a natural course resembling acute myocarditis that progresses to dilated cardiomyopathy in humans.

Viral persistence and its potential role in ongoing myocyte damage were demonstrated in a murine model of Coxsackievirus B3-induced myocarditis using in situ hybridization for the presence of CVB3 genomic RNA[22].

By further examining the sites where viral RNA was detected, Klingel et al.[22] found that in the first 3 days after infection, myocytes containing CVB3 RNA were distributed randomly throughout the myocardium (presumable heterogeneous infection during viraemia). By day 6, infected myocytes were adjacent to foci of inflammatory cells. The numbers of CVB3-infected myocytes were noted from day 6 to 9. This correlated with a significant increase in myocardial injury. After infectious virus could no longer be isolated from the myocardium (from day 15 to 30 post-infection), CVB3 genomes could still be detected in myocardial cells. These positive cells were found primarily within foci of myocardial lesions characterized by fibrosis, myocardial necrosis, and mononuclear cell infiltrates. Interestingly, there was evidence of viral persistence in ACA/SnJ, ABY/SnJ, and SWR/J mice, but not in DBA/1J mice, which were capable of terminating the inflammatory process through elimination of the virus from the heart.

Permissive mouse strains (e.g. A.CA/SnJ, ABY/SnJ, SWR/J) develop ongoing myocarditis after acute infection due to viral persistence, while resistant mouse strains (e.g. DBA/1J and C57Bl/6) eliminate the virus after acute infection. Viral replication in the myocytes with viral persistence has been shown to be restricted at the level of gnomic positive-strand RNA synthesis. In contrast to the acute phase of myocarditis which is characterized by the synthesis of viral positive-strand RNA in great excess, cells with viral persistence contain positive- and negative-strand RNA in approximately the same abundance. Consequently, viral gene expression is decreased in persistently infected cells, reflecting restricted viral RNA synthesis.

VI. Materials and Methods

VI.1. Fourier transform infrared micro-spectroscopy (FTIRM) and imaging (FTIRI):

Fourier transform infrared micro-spectroscopy (FTIRM) and imaging (FTIRI) are techniques that combine light microscopy and infrared spectroscopy[97]. Light microscopy is used to magnify structural detail in samples, while infrared spectroscopy provides information on molecular chemistry.

FTIRM was developed over 20 years ago using a conventional thermal (e.g. globar) infrared light source and a single-element infrared (IR) detector.

It has been used to identify and spatially resolve the chemical makeup of many diverse materials, including various plant and animal tissues, minerals and other geological samples, polymers films and laminates, semiconductors, forensics materials, and pharmaceuticals[98].

The term FTIRI is associated with the recent development of focal plane array (FPA) detectors on IR microscopes[99,100]. The FPA detector consist of an array of IR detector elements that enable spectra of various parts of the sample to be projected on different pixels and collected simultaneously, while the concurrent measurement of all frequencies is retained by the phase modulation of the interferometer. Using a FPA system, the speed at which large IR images can be collected is dramatically improved[97].

When examining the chemical makeup of biological cells and tissues with an infrared (IR) microscope, it is important to achieve sub-cellular spatial resolution. For both FTIRM and FTIRI, the spatial resolution is limited by the wavelengths of infrared (IR) light, which are longer than visible light wavelengths used for conventional optical microscopy. The diffraction-limited spatial resolution is dependent upon the wavelength of light and the numerical aperture (NA) of the focusing optic[101].

In an FTIRI experiment, no physical apertures are used to limit the illumination area of the IR beam. Instead, an array of IR detector elements is used to collect the projected image of the unmasked IR beam on the sample.

An IR spectromicroscope is used, which is designed with 2 paths from the sample to the detector: transmission and reflection.
In transmission mode, the IR light passes through the sample and is collected by a second IR objective that re-collimates the beam and sends it to the IR detector. In reflection mode, the IR light reflects off of the sample and passes back through the illuminating objective. In this configuration, approximately 40-50% of the incident IR light is blocked by a mirror that collects the reflected light[97].

To preserve the original state of the tissue, thin samples (6-10 μm) are prepared by cryogenic sectioning with a microtome, and no embedding material should be used. The cut sections are then planted on an infrared-transparent material with thickness ranging from nanometers to a few micrometers.

VI.2. Experimental animal models and tissue preparation

Mouse models were prepared at Tuebingen University Medical School, Germany. In brief, complementary (cDNA) generated Coxsackievirus B type 3 (CVB3), Nancy strain[102], was grown and propagated in Vero cells (African green monkey kidney cells). Stock virus was prepared by three times freezing and thawing and further purified by sucrose gradient centrifugation. Nine 4 to 5 week-old inbred mice of the strains C57BL/6 and ABY/SnJ (both H-2b) were infected intraperitoneally (i.p.) with 1×10^5 PFU of purified CVB3.
Animals were sacrificed at 4, 8, 28 days post-infection; non-infected animals of the two mouse strains were used as controls. The hearts were removed and frozen in liquid nitrogen.
All animal experiments were carried out in accordance with European and German legal and ethical regulations.

For analysis, 8 μm thick-heart tissue sections were mounted on MirrIR reflective microscope slides (Kevley Technologies, Chesterland, OH) and fixed for 20 minutes at 4 °C in 2% paraformaldehyde before use, which has been shown to preserve cellular components for FTIR microspectroscopy.

For each mouse model (ABY/SnJ and C57BL/6), nine animals were studied; three were used as controls and six were infected with coxsackievirus B3.

The reason for studying the 2 different mouse strains was the evidence of different responses to Coxsackie B virus infection, as mentioned above.

VI.3. FTIR imaging data collection

Data acquisition was performed at The National Synchrotron Light Source (NSLS), New York. IR images were collected using a Perkin Elmer Spectrum Spotlight FTIR Imaging System applying the “image” mode of the instrument. For each tissue section, the entire area of the tissue was defined (approximately 5 mm in diameter) and an IR image was produced for this area using a liquid nitrogen-cooled, 16-pixel mercury cadmium telluride (MCT-A) array detector at a 25 μm pixel resolution. Typically, 5000 -10,000 spectra were collected for each tissue section. In addition, two or three smaller images were collected from each section at higher pixel resolution (6.25 μm). For the high-resolution images, over 100,000 spectra were collected for each tissue section. Using a 25 μm pixel size (4 cm^{-1} resolution, 4 scans/pt.), a 4 mm x 4 mm area of tissue took 110 minutes to image. Using a 6.25 μm pixel size (4 cm-1 resolution, 4 scans/pt.), imaging the same area of tissue would take approximately 29 h to collect.
An absorbance spectrum was recorded for each pixel in trans-reflectance mode. Background spectra were collected from a clean region of the IR-reflective slide. All spectra were collected in the mid-infrared spectral region (4000-720 cm^{-1}). The spectral resolution was 4 cm^{-1} and eight scans were averaged for each spectrum. A visible image of the sample was also collected.
A type I collagen sample (from bovine Achilles tendon, 4 mg/ml in 0.02 M acetic acid)[103] was prepared on a MirrIR microscope slide and used for a collagen reference spectrum. The spectrum was recorded using “point” mode of the Spectrum Spotlight with an aperture of 50 μm x 50 μm, and a spectral resolution of 4 cm^{-1} in the mid IR spectral region (4000-

720 cm^{-1}). The absorbance spectrum was acquired by co-adding 1024 scans in trans-reflectance mode.

VI.4. FTIR imaging data evaluation

Three FTIR spectral regions were used in the data evaluation (Fig. 1): (1) lipid content was determined by integrating the area between 3000 and 2800 cm^{-1} (linear baseline: 3000 - 2800 cm^{-1}), which represents the C—H stretching region and is dominated by the long hydrocarbon chains of lipids; (2) protein content was determined by integrating the amide I band, 1700- 600 (single-point linear baseline at 1800 cm^{-1}), which is assigned to the carbonyl stretching mode of the protein amide backbone (—NH—C═O); (3) collagen content was determined through correlation analysis of the region from 1400 to 1000 cm^{-1} which has a series of absorbance features unique to collagen[106].

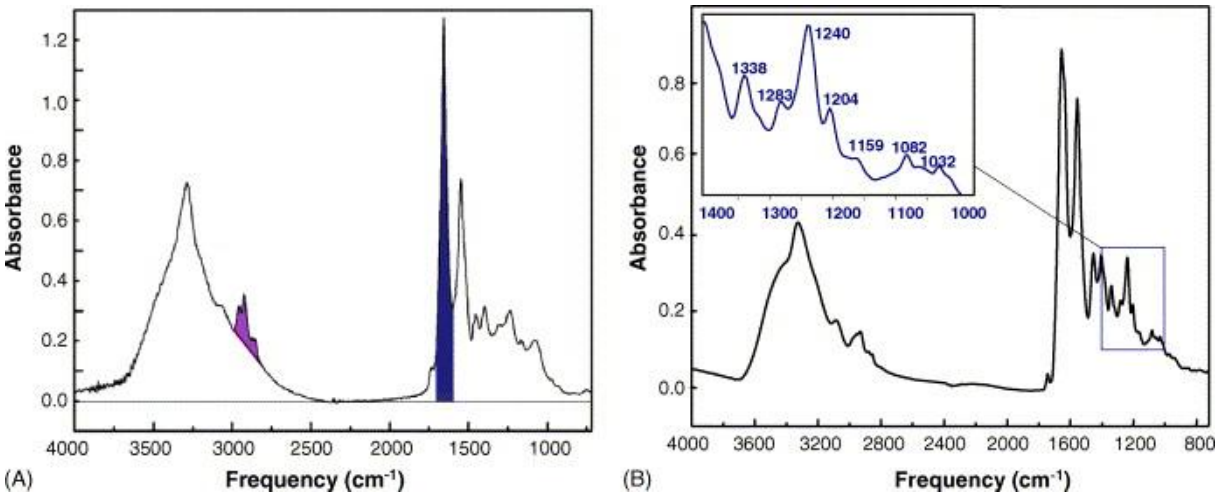

Fig. 1: (A) Infrared spectrum from heart tissue. The lipid/protein (L/P) band ratio is derived from the integrated area ratio between lipid (3000–2800 cm^{-1}) and protein (1700–1600 cm^{-1}). (B) Infrared spectrum of type I collagen. The second derivative of this spectrum was used as a reference spectrum for correlation comparison of collagen content in samples. The insert indicates the spectral region for correlation, i.e. the fingerprint region (1400–1000 cm^{-1}).

Fig. 1A shows a typical IR absorption spectrum of heart muscle tissue. The IR spectrum can be separated into three major regions. The peaks between 3000 and 2800 cm^{-1} are assigned to C—H stretching modes. Specifically, the asymmetric C—H stretching vibrations of the —CH3 and >CH2 fall at ~2959 and ~2921 cm^{-1}, respectively, while the symmetric modes occur at ~2872 and ~2852 cm^{-1}, respectively[107]. This region is a sensitive indicator for lipid content. The absorbance peak centred near 1650 cm^{-1} originates from >C=O stretching vibration of the amide bond backbone in proteins[107]. The exact frequency of this mode depends on the secondary structure of the protein being examined. This peak was used to estimate the concentration of protein in tissue. Collagen content was determined by examining the fingerprint region from 1400 to 1000 cm^{-1}. The spectrum of collagen can be seen in Figure 1B. Collagen absorption features at 1338, 1283, 1240, 1204, 1082 and 1032 cm^{-1} are attributed to CH_2 wagging, CH_3 deformation, C—N stretching and C—OH stretching of collagen[106,108].

The correlation analysis was performed against the reference spectrum of pure type I collagen using the second derivative.

Accordingly, two parameters were established to evaluate the FTIR images in this study: the lipid/protein (L/P) ratio and the collagen content.
Images were plotted with a rainbow colour scale where lowest values were blue and highest values were red. All images for each parameter (L/P ratio and collagen content) were plotted on the same scale for comparison.

To overcome sampling error, many sections from the same tissues were studied. Reproducibility was checked by examining the same section more than one time.

VII. Results

Figure 2 shows the lipid / protein ratio spectral images obtained from the heart tissue sections of the non-infected ABY/SnJ mice and those obtained from infected mice of the same strain at different time points post-infection (4 days, 8 days, and 28 days post infection). The aperture used is 25 µm.

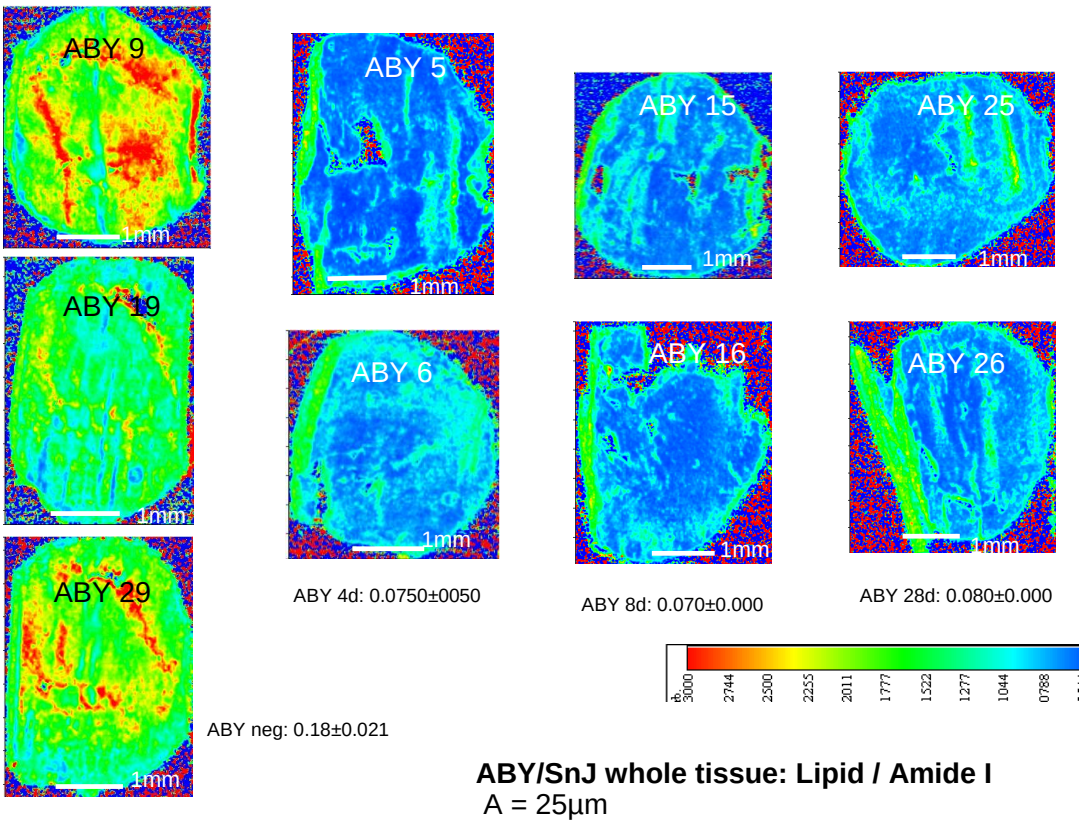

Fig. 2: Lipid / protein ratio images of heart tissue from the ABY/SnJ mouse at different disease stages: control, 4 days, 8 days, and 28 days post-infection (25µm aperture)

Table 1 shows the analysis of the lipid / protein ratio spectra obtained from the heart tissue sections of the non-infected ABY/SnJ mice and those obtained from the heart tissue sections of the non-infected ABY/SnJ mice and those obtained from infected mice of the

same strain at different time points post-infection (4 days, 8 days, and 28 days post-infection). The aperture used is 25 µm.

Table 1: Lipid / protein ratio (L/P) for the whole tissue of mouse strain ABY/SnJ as acquired at 25 µm aperture. (p.i.: post-infection)

Mouse strain	**Non-infected**	**4 days p.i.**	**8 days p.i.**	**28 days p.i.**
ABY/SnJ 1	0.21 ± 0.05	0.07 ± 0.22	0.07 ± 0.49	0.08 ± 0.02
ABY/SnJ 2	0.14 ± 0.66	0.08 ± 0.05	0.07 ± 0.04	0.08 ± 0.03
ABY/SnJ 3	0.19 ± 0.05			
Mean ± SD	0.18 ± 0.021	0.075 ± 0.0050	0.070 ± 0.000	0.080 ± 0.000

Data are presented as mean±SD unless otherwise indicated. An error probability of P<.05 was regarded as significant. Groups were compared using the Kruskal-Wallis ANOVA on ranks, and P was shown to be 0.022.

Figure 3 shows the lipid / protein ratio spectral images obtained from the heart tissue sections of the non-infected C57BL/6 mice and those obtained from infected mice of the same strain at different time points post infection (4, 8, and 28 days post infection). The aperture used is 25 µm

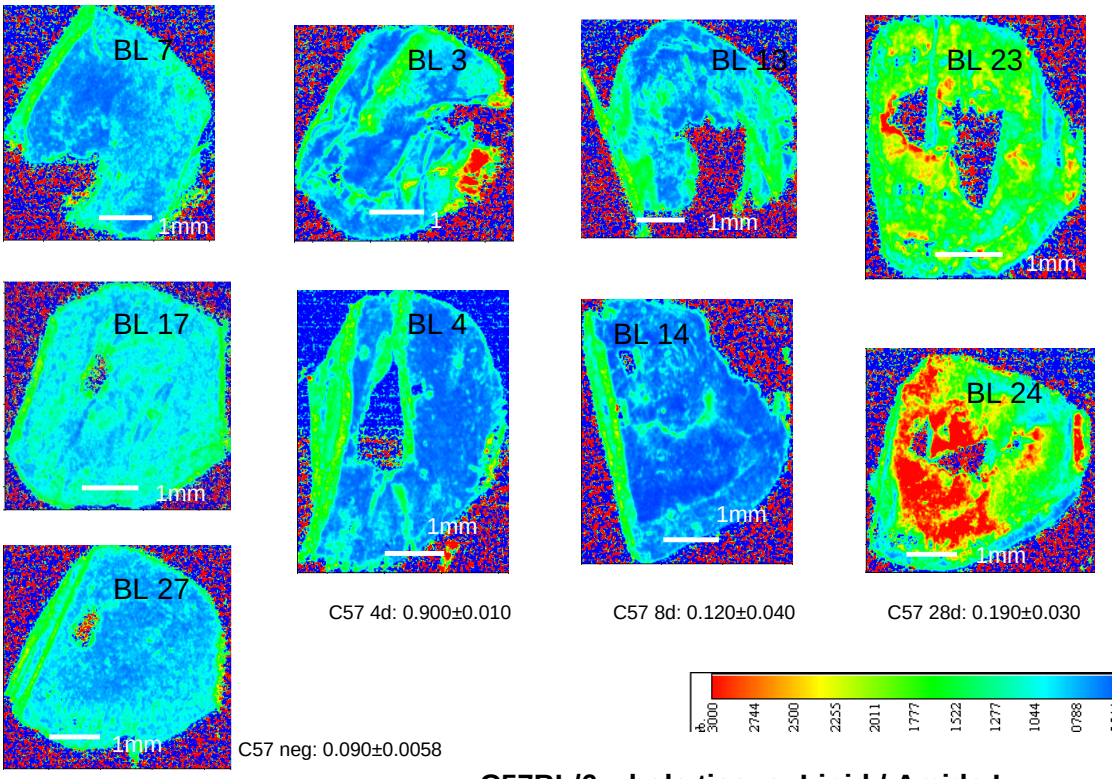

C57BL/6 whole tissue: Lipid / Amide I

A = 25µm

Fig. 3: Lipid / protein ratio images from the C57BL/6 (25 µm aperture) mouse at different disease stages: control, 4 days, 8 days, and 28 days post infection

Table 2 shows the analysis of the L / P ratio spectra obtained from the heart tissue sections of the non-infected C57BL/6 mice and those obtained from infected mice of the same strain at different time points post infection (4, 8, and 28 days post infection). The aperture used is 25 µm

Table 2: Lipid / protein ratio (L/P) for the whole tissue of mouse strain C57BL/6 as aquired at 25 µm aperture. (p.i.: post-infection)

Mouse strain	**Non-infected**	**4 days p.i.**	**8 days p.i.**	**28 days p.i.**
C57BL/6 1	0.08 ± 0.03	0.10 ± 1.32	0.08 ± 0.29	0.22 ± 8.98
C57BL/6 2	0.10 ± 0.03	0.08 ± 0.30	0.16 ± 0.22	0.16 ± 5.99
C57BL/6 3	0.09 ± 0.05			
Mean ± SD	0.090 ± 0.0058	0.09 ± 0.010	0.120 ± 0.040	0.190 ± 0.030

Data are presented as mean±SD unless otherwise indicated. An error probability of P<.05 was regarded as significant. Groups were compared using the Kruskal-Wallis ANOVA on ranks, and P was shown to be 0.031.

Figure 4 shows the lipid / protein ratio spectral images obtained from the heart tissue sections of the non-infected ABY/SnJ mice and those obtained from infected mice of the same strain at different time points post infection (4, 8, and 28 days post infection). The aperture used is 6.25 µm.

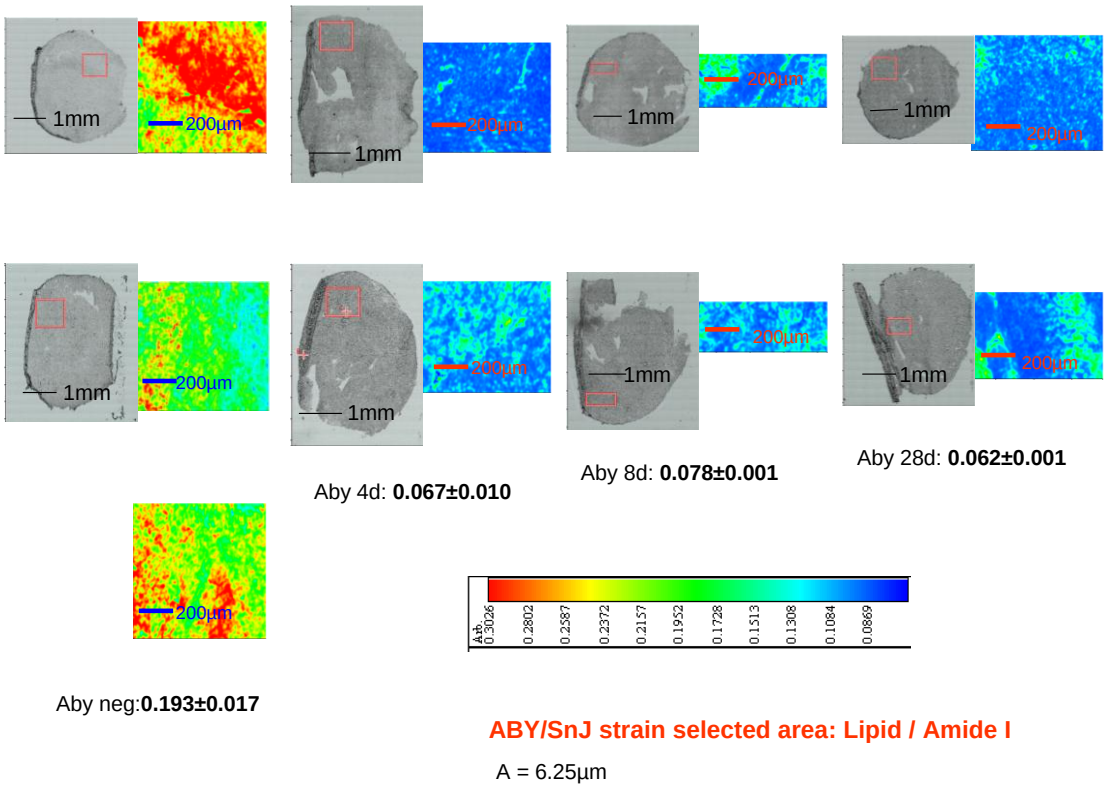

Fig. 4: Lipid / protein ratio images of heart tissue from the ABY/SnJ mouse at different disease stages: control, 4 days, 8 days, and 28 days post infection (6.25 µm aperture)

Table 3 shows the analysis of the L / P ratio spectra obtained from the heart tissue sections of the non-infected ABY/SnJ mice and those obtained from infected mice of the same

strain at different time points post infection (4, 8, and 28 days post infection). The aperture used is 6.25 µm.

Table 3: Lipid / protein ratio (L/P) for the whole tissue of mouse strain ABY/SnJ as aquired at 6.25 µm aperture. (p.i.: post infection)

Mouse strain	**Non-infected**	**4 days p.i.**	**8 days p.i.**	**28 days p.i.**
ABY/SnJ 1	0.21 ± 0.012	0.057 ± 0.0055	0.077 ± 0.0092	0.061 ± 0.0052
ABY/SnJ 2	0.16 ± 0.018	0.077 ± 0.0088	0.078 ± 0.009	0.063 ± 0.0049
ABY/SnJ 3	0.21 ± 0.012			
Mean ± SD	0.193 ± 0.017	0.067 ± 0.010	0.078 ± 0.001	0.062 ± 0.001

Data are presented as mean±SD unless otherwise indicated. An error probability of P<.05 was regarded as significant. Groups were compared using the Kruskal-Wallis ANOVA on ranks, and P was shown to be 0.026.

Figure 5 shows the lipid / protein ratio spectral images obtained from the heart tissue sections of the non-infected C57BL/6 mice and those obtained from infected mice of the same strain at different time points post infection (4, 8, and 28 days post infection). The aperture used is 6.25 µm.

Table 4: Lipid / protein ratio (L/P) for the whole tissue of mouse strain C57BL/6 as acquired at 6.25 µm aperture. (p.i.: post infection)

Mouse strain	Non-infected	4 days p.i.	8 days p.i.	28 days p.i.
C57BL/6 1	0.0766 ± 0.0086	0.089 ± 0.011	0.067 ± 0.0078	0.159 ± 0.018
C57BL/6 2	0.097 ± 0.011	0.057 ± 0.0060	0.058 ± 0.0064	0.294 ± 0.0165
C57BL/6 3	0.069 ± 0.0076			
Mean ± SD	0.078 ± 0.010	0.087 ± 0.032	0.062 ± 0.005	0.211 ± 0.053

Data are presented as mean±SD unless otherwise indicated. An error probability of P<.05 was regarded as significant. Groups were compared using the Kruskal-Wallis ANOVA on ranks, and P was shown to be 0.045.

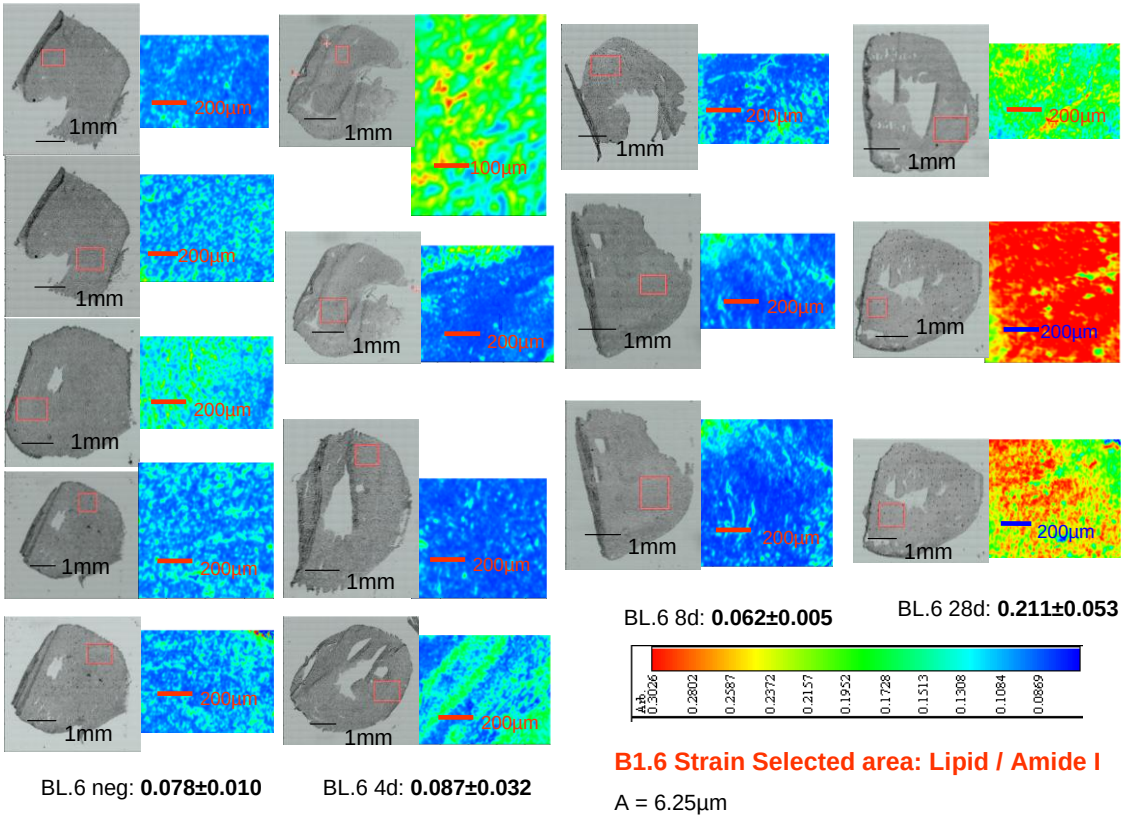

Fig. 5: Lipid / protein ratio images of heart tissue from the C57BL/6 mouse at different disease stages: control, 4 days, 8 days, and 28 days post infection (6.25 µm aperture)

Table 4 shows the analysis of the lipid / protein ratio obtained from the heart tissue sections of the non-infected C57BL/6 mice and those obtained from infected mice of the same strain at different time points post infection (4, 8, and 28 days post infection). The aperture used is 6.25 µm.

Figure 6 shows the collagen correlation images obtained from heart tissue sections of the non-infected ABY/SnJ mice and those obtained from infected mice of the strain at different time points post infection (4, 8, and 28 days post infection). The aperture used is 25 µm.

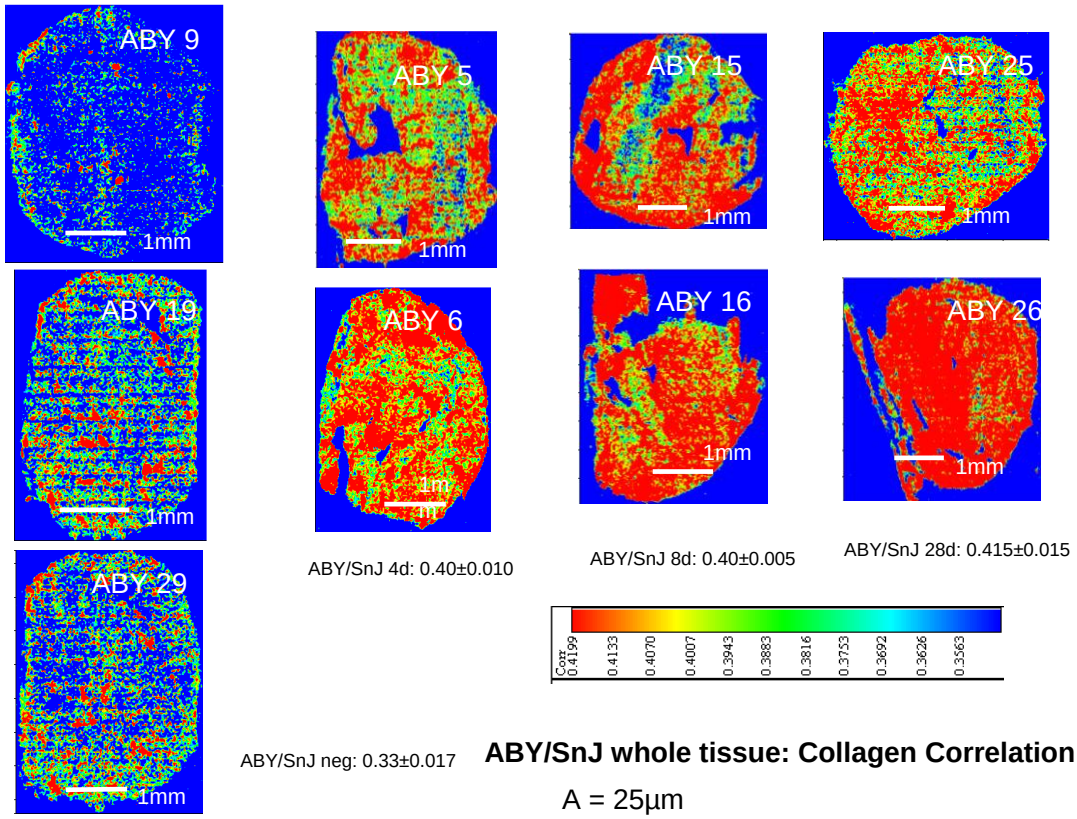

Fig. 6: Collagen correlation images of heart tissue from the ABY/SnJ mouse at different disease stages: control, 4 days, 8 days, and 28 days post infection (25 µm aperture)

Table 5 shows the analysis of collagen correlation (CC) obtained from heart tissue sections of the non-infected ABY/SnJ mice and those obtained from infected mice of the strain at different time points post infection (4, 8, and 28 days post infection). The aperture used is 25 µm.

Table 5: Collagen correlation (CC) for the whole tissue of mouse strain ABY/SnJ as acquired at 6.25 µm aperture. (p.i.: post infection)

Mouse strain	Non-infected	4 days p.i.	8 days p.i.	28 days p.i.
ABY/SnJ 1	0.30±0.08	0.39±0.08	0.40±0.07	0.40±0.05
ABY/SnJ 2	0.35±0.08	0.41±0.08	0.41±0.07	0.43±0.06
ABY/SnJ 3	0.35±0.07			
Mean ± SD	0.33 ± 0.017	0.40 ± 0.010	0.40 ± 0.0050	0.415 ± 0.015

Data are presented as mean±SD unless otherwise indicated. An error probability of P<.05 was regarded as significant. Groups were compared using the Kruskal-Wallis ANOVA on ranks, and P was shown to be 0.001.

Figure 7 shows the collagen correlation images obtained from heart tissue sections of the non-infected C57BL/6 mice and those obtained from infected mice of the strain at different time points post infection (4, 8, and 28 days post infection). The aperture used is 25 µm.

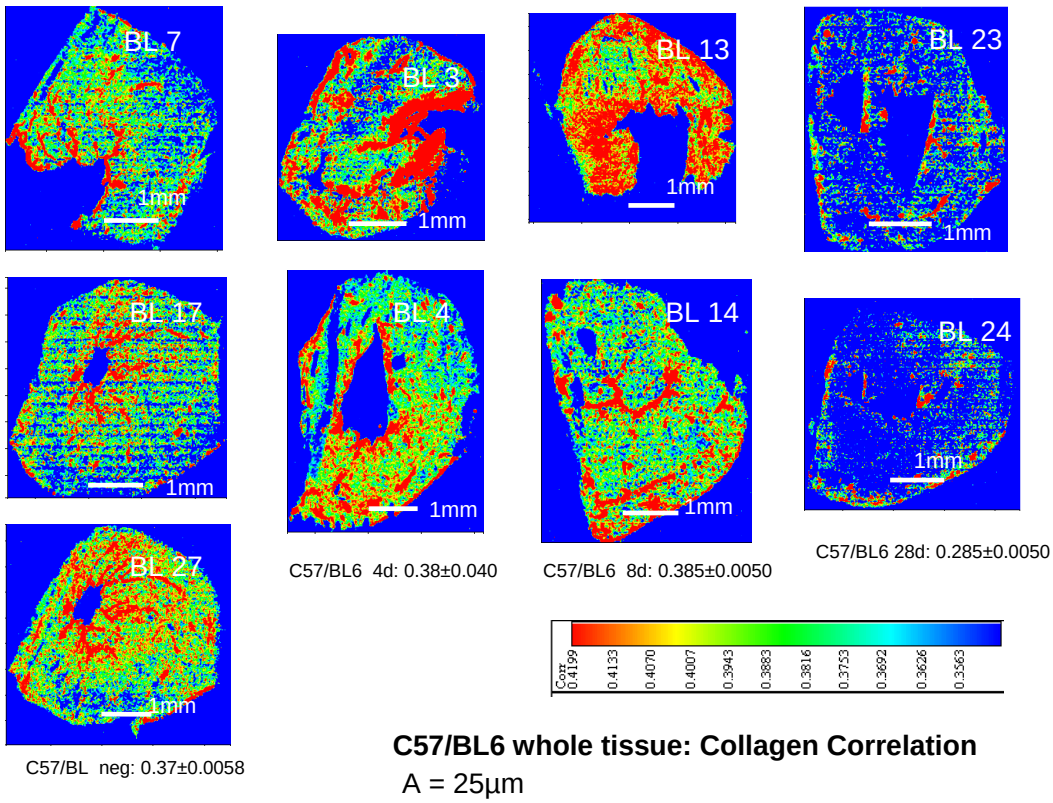

Fig. 7: Collagen correlation images of heart tissue from the C57BL/6 mouse at different disease stages: control, 4 days, 8 days, and 28 days post-infection (25 µm aperture)

Table 6 shows the analysis of collagen correlation (CC) spectra obtained from heart tissue sections of the non-infected C57BL/6 mice and those obtained from infected mice of the strain at different time points post infection (4, 8, and 28 days post infection). The aperture used is 25 µm.

Table 6: Collagen correlation (CC) for the whole tissue of mouse strain C57BL/6 as acquired at 25 µm aperture. (p.i.: post infection)

Mouse strain	Non-infected	4 days p.i.	8 days p.i.	28 days p.i.
C57BL/6 1	0.37±0.06	0.42±0.14	0.39±0.06	0.29±0.12
C57BL/6 2	0.37±0.06	0.34±0.12	0.38±0.06	0.28±0.11
C57BL/6 3	0.38±0.07			
Mean ± SEM	0.37 ± 0.0058	0.38 ± 0.040	0.385 ± 0.0050	0.285 ± 0.0050

Data are presented as mean±SD unless otherwise indicated. An error probability of P<.05 was regarded as significant. Groups were compared using the Kruskal-Wallis ANOVA on ranks, and P was shown to be 0.031

Figure 8 shows the collagen correlation images obtained from heart tissue sections of the non-infected ABY/SnJ mice and those obtained from infected mice of the same strain at different time points (4, 8, and 28 days postinfection). The aperture used is 6.25 µm.

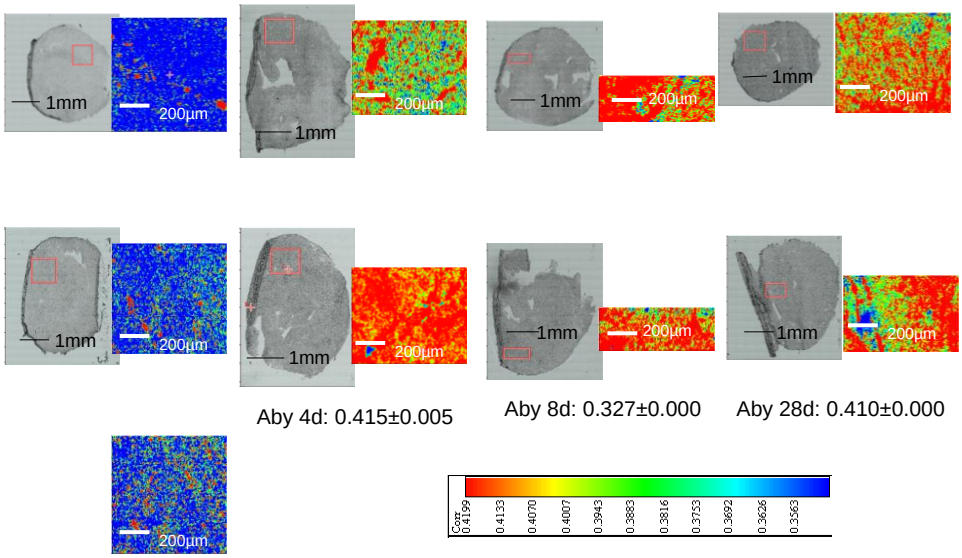

Fig. 8: Collagen correlation images of heart tissue from the ABY/SnJ mouse at different disease stages: control, 4 days, 8 days, and 28 days post infection (6.25 µm aperture)

Table 7 shows the numerical analysis of collagen correlation images obtained from heart tissue sections of the non-infected ABY/SnJ mice and those obtained from infected mice of the same strain at different time points (4, 8, and 28 days post infection). The aperture used is 6.25 µm.

Table 7: Collagen correlation (CC) for the whole tissue of mouse strain ABY/SnJ as acquired at 6.25 µm aperture. (p.i.: post infection)

Mouse strain	Non-infected	4 days p.i.	8 days p.i.	28 days p.i.
ABY/SnJ 1	0.295±0.0976	0.4046±0.0551	0.4395±0.0592	0.4168±0.0424
ABY/SnJ 2	0.342±0.07237	0.4267±0.0573	0.4336±0.06804	0.4135±0.0483
ABY/SnJ 3	0.3501±0.08023			
Mean ± SD	0.3292±0.01701	0.4157±0.0111	0.4366±0.0029	0.4152±0.0017

Data are presented as mean±SD unless otherwise indicated. An error probability of P<.05 was regarded as significant. Groups were compared using the Kruskal-Wallis ANOVA on ranks, and P was shown to be 0.002.

Table 8 shows the numerical analysis of collagen correlation images obtained from heart tissue sections of the non-infected C57BL/6 mice and those obtained from infected mice of the same strain at different time points (4, 8, and 28 days post infection). The aperture used is 6.25 µm.

Table 8: Collagen correlation (CC) for the whole tissue of mouse strain C57BL/6 as acquired at 6.25 µm aperture. (p.i.: post infection)

Mouse strain	Non-infected	4 days p.i.	8 days p.i.	28 days p.i.
C57BL/6 1	0.3956±0.0372 0.3429±0.05941	0.4030±0.0743 0.3776±0.0672	0.3865±0.0514	0.3737±0.0720
C57BL/6 2	0.3815±0.05122	0.4199±0.0482 0.4016±0.0673	0.4130±0.0451 0.3829±0.0549	0.2602±0.0861 0.1663±0.0637
C57BL/6 3	0.4084±0.0348 0.3684±0.0654			
Mean ± SD	0.3797±0.0056	0.4005±0.0102	0.3922±0.0057	0.2935±0.0802

Data are presented as mean±SD unless otherwise indicated. An error probability of P<.05 was regarded as significant. Groups were compared using the Kruskal-Wallis ANOVA on ranks, and P was shown to be 0.003.

Enteroviruses have been shown to induce an acute inflammation of the myocardium with or without cardiac dysfunction (myocarditis / inflammatory cardiomyopathy) that can transform to virus-negative cardiomyopathy. The three phases generally involved in this disease are: early, acute, and chronic stages. Extracellular matrix remodeling plays a significant role in cardiac dysfunction. Lipid replacement by collagen deposition has been recognized as one of major indicators in the progression of cardiac dysfunction[104,105], and infrared imaging can be used to detect both collagen and lipid in the disease[103].

By analysing the lipid / protein ratio and collagen correlation data obtained throughout the progression of the disease in every mouse strain and comparing these with the composition of the heart tissue section in the non-infected state, it becomes apparent that the extracellular matrix plays a significant role in the transform to the chronic cardiomyopathy.
The changes in the extracellular matrix are reliably depicted by infra-red spectromicroscopy.

Figure 9 shows FTIR images for the permissive mouse strain (ABY/SnJ) at different disease stages: early (4th day post-infection), acute (8th day post-infection) and chronic (28th day post-infection). The collagen distribution can be seen in Figure 9A, as determined by the collagen correlation from 1400 to 1000 cm^{-1}. All images are plotted on the same scale. Results show that the diseased tissue has a higher correlation with the pure collagen reference spectrum, indicating that collagen levels are elevated in this tissue compared to the control tissue. Specifically, the collagen correlation coefficients are 0.416 ± 0.011, 0.437 ± 0.003, and 0.415 ± 0.002, in the early, acute, and chronic stages, respectively, while in control tissue it is 0.329 ± 0.017. Both correlation maps and the coefficient averages indicate there is no significant difference among three disease stages but a 26% increase was found in the collagen correlation for the diseased tissue relative to the control. In addition, the FTIR images show that there is a uniform distribution of collagen deposition in the diseased tissue; it is not a localized effect. This is supported by low standard deviations for the correlation coefficients (Table 9).

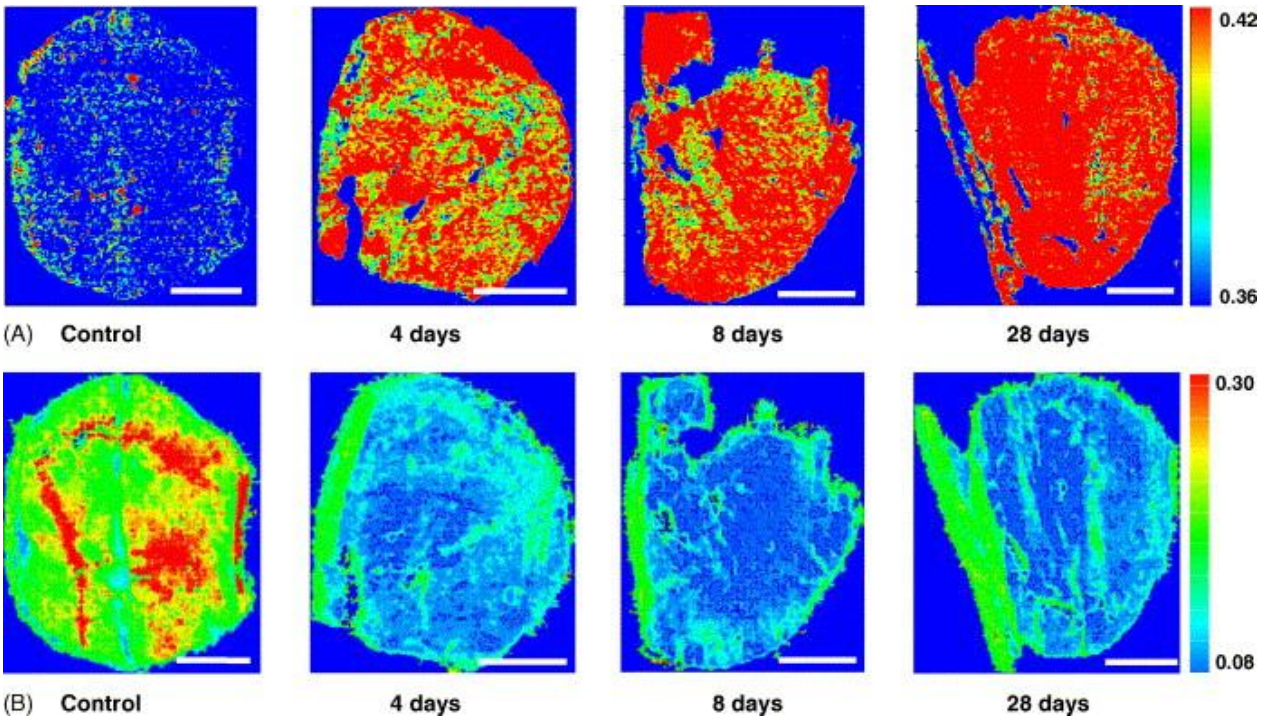

Fig. 9.(A) Collagen correlation images and (B) lipid/protein ratio images of heart tissue from the ABY/SnJ mouse model at different disease stages: control, 4 days, 8 days, and 28 days post infection. The collagen correlation was calculated using the second derivative spectrum of Type I collagen from 1400 to 1000 cm^{-1}. Data collection conditions: pixel size=25 μm, spectral resolution= 4 cm^{-1}, scan number=8 scans/pixel. The scale bar represents 1.0 mm.

Table 9: Lipid/protein ratio and collagen correlation: means ± S.E.M

Disease stage	Control	4 days	8 days	28 days
ABY/SnJ				
CC	0.329 ± 0.017	0.0416 ± 0.011	0.437 ± 0.003	0.415 ± 0.002
L/P	0.193 ± 0.017	0.067 ± 0.000	0.078 ± 0.001	0.062 ± 0.001
C57BL/6				
CC	0.380 ± 0.006	0.401 ± 0.010	0.392 ± 0.006	0.294 ± 0.080
L/P	0.078 ± 0.010	0.087± 0.032	0.062 ± 0.005	0.211± 0.053

The L/P ratio is seen in Figure 9B. As can be seen, a high L/P ratio exists for the control tissue (0.193 ± 0.017), and the L/P ratio is more than three times lower in all three stages

of infected tissue: 0.067 ± 0.010, 0.078 ± 0.001, and 0.062 ± 0.001 for early, acute and chronic stages, respectively. No significant differences were observed between the three diseased stages. Since these data are reported as ratios to account for any sample thickness variations, these results could indicate that the diseased states possess either a higher protein content and/or a lower lipid level. However, the increased collagen content is observed in the diseased stages, strongly suggesting that protein content is increasing. In addition, the CH_2/CH_3 ratio can be applied to indicate lipid content, where a higher ratio indicates longer-chained lipids and a higher lipid content[103].
In these studies, the infected tissue had CH_2/CH_3 ratios comparable as the control tissue, supporting the conclusion that the lower L/P ratio in the diseased states comes from elevated protein (i.e. collagen) and not a significant reduction in lipid content.

For the C57BL/6 strain, the collagen distribution and L/P ratio images are shown in Figures 10A and B, respectively, plotted on the same colour scales as in Figures 9A and B. No differences were observed in collagen correlation between the control (0.380 ± 0.006), 4 days post-infection (0.401 ± 0.010), and 8 days post-infection (0.392 ± 0.006) tissue. Similarly, the L/P ratio did not differ significantly between the control (0.078 ± 0.010), 4 days post-infection (0.087 ± 0.032), and 8 days post-infection (0.062 ± 0.005) tissue. However, a dramatic reduction in collagen content (0.294 ± 0.080) and increased L/P ratio (0.211 ± 0.053) were observed in the 28 days post-infection tissue.

These results suggest that C57BL/6 strain can recover from the CVB3 infection during the acute phase of disease. In addition, the original (control) composition of the C57BL/6 strain differs from the ABY/SnJ strain; the C57BL/6 strain has a higher collagen content and a lower L/P ratio than the ABY/SnJ strain. These differences may influence the ability of the C57BL/6 strain to stabilize the disease and initiate recovery.

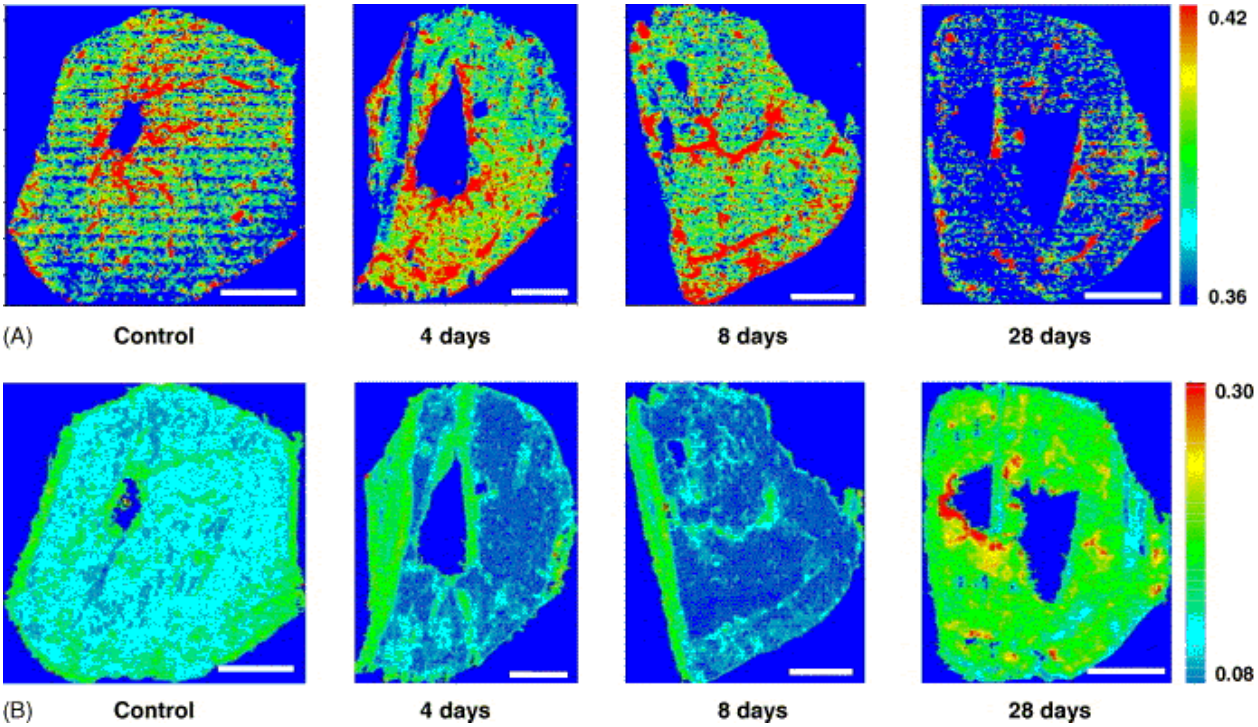

Fig.10: (A) Collagen correlation images and (B) lipid/protein band ratio maps of heart tissue from the C57BL/6 mouse models at different disease stages: control, 4 days, 8 days, and 28 days post infection. The collagen correlation was calculated using the second derivative spectrum of type I collagen from 1400 to 1000 cm^{-1}. Data collection conditions: pixel size = 25 μm, spectral resolution = 4 cm^{-1}, scan number = 8 scans/pixel. The scale bar represents 1.0 mm.

For both the ABY/SnJ and C57BL/6 strains, a strong inverse correlation was observed between the collagen content and the L/P ratio (Figure. 11). This is reflected in the negative slopes for the two linear relationships: -0.70 (ABY/SnJ) and -0.73 (C57BL/6), plotted on a scale from 0 to -1, representing the lowest to highest correlation. The linear regressions, r^2, of the two lines were 0.82 (ABY/SnJ) and 0.64 (C57BL/6).

Thus, as collagen concentration increases, the L/P ratio decreases, suggesting that extracellular matrix remodeling, i.e. collagen deposition, replaces normal tissue as the CVB3 infection induces myocarditis.

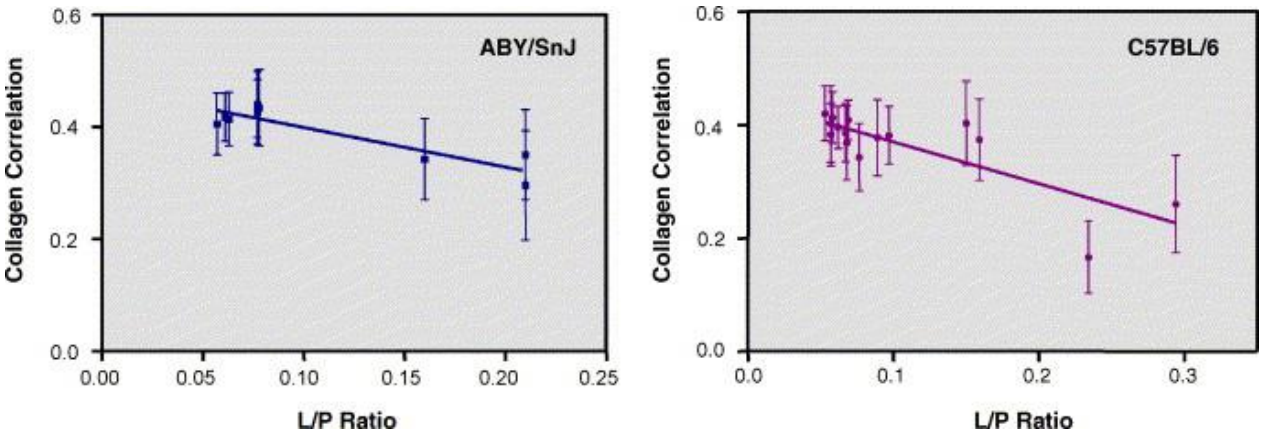

Fig. 11: Linear correlation between the lipid/protein ratio and the collagen correlation in the (left) ABY/SnJ and (right) C57BL/6 strains. Means and S.E.M.s were calculated using data collected at a pixel size of 6.25 μm, spectral resolution= 4 cm^{-1}, scan number= 8 scans/pixel.

These findings are consistent with numerous previous studies on CVB3 viral myocarditis using murine models. Specifically, ABY/SnJ(H-2^b) is classified as a permissive host prone to sustaining chronic inflammation of myocarditis by CVB3-infection; C57BL/6(H-2^b) is a resistant host, which usually eliminates CVB3 during acute myocarditis, preventing the development of chronic myocarditis[109].

VIII. Discussion

Heart failure, a syndrome associated with a greatly heightened risk of death, is characterized by abnormalities of cardiac function with the inability of the heart to pump blood at an output sufficient to meet the requirements of the metabolizing tissues or the ability to do so only at abnormally elevated diastolic pressure or volume. Both the incidence and prevalence of heart failure are growing. The annual incidence of new cases of heart failure rises from less than 1 per 1000 patient-years among those younger than 45 years of age, to 10 per 1000 patient-years among those older than 65 year, to 30 per 1000 patient-years (3%) for patients older than 85 years. Prevalence figures are also exponentially increasing from 0.1% before 50 to 55 year of age to almost 10% after the age of 80 years[110]

Any condition that causes myocardial necrosis of produces chronic pressure or volume overload can lead to myocardial dysfunction and heart failure.

Cardiomyopathy, a disease of heart muscle, is causal for heart failure in approximately 7% of all congestive heart failure patients[111]. For descriptive rather than etiologic purposes, cardiomyopathies are designated as dilated, hypertrophic, or restrictive.

Dilated cardiomyopathy is characterized by thinning of the left ventricular wall and dilatation of the ventricles, resulting in a reduction of the ejection volume from the heart. This causes serious arrhythmias (inflammatory infiltrates may act as arrhythmogenic foci leading to sudden cardiac death in the absence of clinical heart failure) and thromboembolic events, explaining the substantial mortality rate of this disease. Histopathological investigations have shown that there is a moderate myocyte hypertrophy and death, along with replacement fibrosis[112] Dilated cardiomyopathy is preceded in a significant proportion of patients with myocardial inflammation (myocarditis)[34].

Myocarditis is a heterogeneous final common pathway for non ischemic inflammation of the myocardium of diverse aetiologies[113]. It is a common indication of listing

for cardiac transplantation[114], and a significant cause of unexplained sudden cardiac death in young patients[115].

The causes of myocarditis include a broad range of viral, bacterial, and fungal infections, systemic and collagen vascular diseases, drugs, and toxins. The most common viral agents detected by myocardial genome PCR in biopsy-proven acute myocarditis comprise the enteroviruses of the family Picornaviridae, in particular Coxsackie B viruses, which have been established as highly prevalent human pathogens.

The gold standard for the detection of myocardial inflammation (myocarditis) remains direct visualization of affected myocardium by either endomyocardial biopsy or autopsy. The diagnosis of myocarditis is based on the presence of inflammatory cells in the heart and can be classified by the Dallas or Marburg criteria[116,117,118,119]. These criteria define active or definitive myocarditis by the amount of inflammatory infiltrate in the myocardium, whereas cases with fibrosis accompanied by lesser degrees of inflammation are considered chronic, borderline, persistent (ongoing), and healing (resolving) myocarditis.
Endomyocardial biopsy specimens are considered diagnostic of myocarditis if light microscopy reveals evidence of both infiltrating lymphocytes and myocytolysis[59].

Owing to its often insidious onset and highly variable clinical presentation, the real incidence and prevalence of histologic myocarditis is unknown. Myocarditis is detected in 1-9% of routine postmortem examinations[120].

Prognosis of biopsy-proven acute myocarditis relates not only to clinical manifestations at onset, but also to histologic classification and biomarkers[113]. Studies of cellular apoptotic pathways show that serum levels of Fas and Fas ligands are elevated in patients with acute myocarditis compared with those in controls, and in fatal cases, compared with survivors of acute mocarditis[121]. Patients with fulminant myocarditis progressing to cardiogenic shock or death have demonstrated significantly elevated levels of serum interleukin-10 [IL-10][122]. The next highest predictor of minimal recovery of left ventricular ejection fraction (LVEF) at 6 and 12 months is the elevated of Fas and tumour necrosis

factor alpha (TNF-α)-receptor 1 expression[123]. Similarly, the presence of antimyosin autoantibodies (AMAAB) in patients with biopsy-proven myocarditis predicted failure of LVEF to recover, a decline in stroke volume index (SVI), and increased myocardial stiffness at 6 months[124]

Recently, persistent viral genome expression of enterovirus, adenovirus, parvovirus B19, and HHV-6 have been associated with progressive impairment in left ventricular ejection fraction; while spontaneous elimination by the host correlated with significant recovery of LVEF in patients with biopsy-proven viral myocarditis[125]. Coxsackie B3 viral myocardial infection in CD4 T-cell deficient major histocompatibility complex (MHC) class II knockout mice and IL-4 knockout mice show heavy myocardial fibrosis after severe acute myocarditis, which develops between day 7 and day 21 post-infection[126].

The cardiac connective tissue, a major component of the extracellular matrix, has an important supportive role by surrounding the various types of cells found in the heart and binding them to each other so that the force transmission is uniform throughout the myocardium. The connective tissue is produced largely by fibroblastic cells and contains collagen as well as other important matrix proteins such as laminin. Fibroblasts are the most abundant cells found in the myocardium. This underscores the importance of the extracellular matrix. This network also helps translate signals induced by mechanical stress into signals promoting cell growth. Thus, the extracellular matrix participates in the remodeling of the myocardium that accompanies left ventricular hypertrophy and heart failure. Fibrillar collagen types I and III are the most abundant proteins in the interstitial space[127], with the ratio of type I to type III of approximately 1.3:1 to 1.9:1[128]. Collagen fibres extend from the surface of the cells to the tissue skeleton as well as from cell to cell. These fibres act as “struts” to hold the myofibrils in position so that the pattern of conduction is orderly[129]. In physiological amounts, collagen may help to limit the degree of ventricular dilatation when it is increased in proportion to the degree of myocardial hypertrophy. In contrast, excessive collagen in disease states (e.g. ischemia) leads to decreased compliance and increased chamber stiffness or reduced distensibility. The clinical result is poor relaxation, and hence, a diastolic heart failure. However, for left ventricular dilatation

to occur, “myocyte slippage” is required[129]. This in turn means weakening of the extracellular matrix, thereby allowing “remodelling” with myocyte slippage and dilatation of the left ventricle[130].

Remodeling describes the time-dependent and often insidious structural alterations, whereby the relationship of the ventricular cavity volume increases out of proportion to mass. The distorted global ventricular geometry, with the ellipsoid-shaped ventricle becoming more spherical, is accompanied by changes in the myocardial interstitium that lead to altered orientation of the myofibrils and progressive fibrosis. The result is further deterioration of cardiac contractile performance.

During cardiac remodeling, two broad groups of alterations are encountered: alterations in the myocyte component, and alterations in the extracellular matrix component[128]. The myocardium undergoes progressive myocyte loss through necrosis, apoptosis, or autophagy. The changes in the extracellular matrix include changes in the fibrillar collagen synthesis and degradation, changes in the degree of collagen cross-linking, and the loss of collagen struts that connect the individual cardiac myocytes[131].
Markers of collagen turnover have been shown to be increased in patients with dilated cardiomyopathy compared with age-matched control subjects[131].

Progressive left ventricular remodeling is shown to be directly related to future deterioration in left ventricular performance and a less favourable clinical course in patients with heart failure[132].

The pathogenesis of myocarditis represents a classic model of cardiac injury followed by host immune response in the form of cardiac inflammation. The outcome is critically dependent on the virulence of the causative agent, the host immune system, and the ability of the host to effectively repair the ensuing injury[35]

The commonest viral triggers are Coxsackie virus, adenovirus, parvovirus, and hepatitis C virus. Coxsackieviruses are single-stranded RNA viruses that have natural tropism for gut

epithelial cells, immune cells, neurons, and cardiomyocytes. All strains of Coxsackieviruses gain entry into the myocardium through the coxsackie-adenovius receptor134. To facilitate entry into cells, Coxsackievirus produces protease 2A, a cysteine endopeptidase that can cleave the dystrophin-sarcoglycans complex, which is responsible for the linkage of myocyte cytoskeleton to the extracellular matrix[135]. A recent study provided significant proof that the production of this cytoskeleton-modifying protease is sufficient to produce dilated cardiomyopathy[136], which can be interpreted as direct remodeling effect of the virus on the myocardium, through cleavage of the dystrophin-sarcoglycans complex and sacrolemmal disruption. On the other hand, the virus can also trigger innate immunity, which helps the host fight against the infection; for example, through activation of signalling for survival (STAT3 and gp130), and systemic clearance of the virus (interferon regulator factor-3)[35].

This immune response can be exuberant, leading to myocardial destruction and myocyte loss. However, an inadequate host immune response results in cardiac remodeling, leading to dilated cardiomyopathy[133].

Thus, monitoring the distribution and concentration of collagen during the different stages of Coxsackievirus B3-induced viral myocarditis in different immunocompetent mouse strains will contribute to the thorough understanding of disease progression.

Murine myocarditis may be conceptualized in three phases: (1) viremia and direct injury up to day 3 post-infection; (2) inflammatory response from day 5 to day 14 post-infection; and (3) variable degrees of reparation and remodelling after 14 days post-infection[37]. Major determinants of long-term heart failure are the degree of cardiac tissue loss by apoptotic or necrotic mechanisms and cardiac remodeling following these damages.

Virus-induced myocytolysis occurs early in the infective period and despite viral clearance, ongoing inflammation may still occur, thus aggravating the disease by influencing cardiac restructuring and cell death events.

Detection of changes in the extracellular matrix has been traditionally achieved by dichrome staining, Western blot analysis, immunohistochemistry, Northern analysis, tissue 4-hydroxyproline concentration, and scanning electron microscopy. Despite the many advantages of these techniques, shortcomings in the detection of spatial distribution of organ collagens are well recognized[23].

The current work applied infrared spectromicroscopy in order to provide an alternative means of analysing collagen spatial distribution in murine models of Coxsackievirus B3-induced myocarditis.

In Fourier transform infrared spectromicroscopy, as covalent bonds vibrate, they absorb energy in the form of IR light. The wavelength of the light that is absorbed depends on the nature of the covalent bond (e.g. C=O, N-H), the type of vibration (bending, stretching, etc.), and the environment of the bond. The IR spectrum of a tissue sample can be regarded as a molecular fingerprint of the tissue. If this molecular fingerprint is modified by a disease process, then IR spectromicroscopy can be used to detect and monitor that process[137].

Infrared spectroscopy alone does not reveal the spatial distribution of tissue collagen. With IR microscopy, however, the microscope functions in much the same way as does a normal light microscope, except that it uses IR light instead of visible light[137]. The IR microscope acts as a beam condenser, focusing the normally broad IR beam onto a much narrower area of the microtomed tissue. By varying the size of aperture, tissue sections can be spectroscopically mapped with a spatial resolution as high as 10 x 10 μm.

Using this technique, this study demonstrated that in the acute phase of mouse model of CVB3-induced myocarditis, collagen content increases and L/P ratio decreases in both the permissive (ABY/SnJ) and resistant (C57BL/6) strains of CVB3-infected mice. This effect has been shown to be broadly distributed within the tissue, and not occurring in a localized fashion. However, in the chronic stage of the disease, the above mentioned changes persist only in the permissive (ABY/SnJ) strain.

This is consistent with the postulation that Coxsackievirus infection produces two different immune responses in affected immunocompetent hosts that occur along with spontaneous elimination of the virus by the resistant host and the viral persistence in the permissive host, with the progression to chronic disease.

The results of this study also show that the two strains have different compositions of the extracellular matrix in the uninfected state, which may provide an insight into the mechanism for the different responses. Previous studies have shown that the composition of extracellular matrix in the uninfected members of the same strain does not change at different time points.

The changes in the collagen correlation and L/P ratio in the different strains reflect the shift towards cardiac remodeling and the development of chronic, dilated cardiomyopathy in the permissive strain.

The method used in this work, however, is limited by the inability to measure the absolute amount of each component of the extracellular matrix exactly. It is also only applied in vitro and on specially prepared specimens. Moreover, it is effort-, and time-consuming. With the development of more sophisticated microscopes and easy-to-apply methods for data analysis and interpretation, more can be gained on the wake of understanding the pathogenesis of viral myocarditis. This may help in developing new predictive tools for the prognosis, as well in refining the therapeutic approaches that are already available and aids in the development of new therapeutic modalities.

IX. Summary

Coxsackievirus B3 (CVB3), a member of the Picornaviridae family, is the leading cause of viral myocarditis, of which dilated cardiomyopathy (DCM) is a major sequela. Both direct viral and immune-mediated mechanisms have been shown to contribute to the pathogenesis of acute injury and subsequent cardiac remodelling. As the disease progresses, changes in both the myocytes and the extracellular matrix are detected.

In addition to the myocytes, fibroblasts, and vasculature, the myocardium contains also a gel-like extracellular matrix (ECM)[50]. The extracellular matrix consists of collagens, proteoglycans, basal laminae, fibronectin, laminin, osteopontin, and other molecules. The ECM provides the myocardium with the structural integrity and alignment critical for pressure distribution and contractility, as well as cell growth, differentiation, and survival.

Most of the interstitial matrix proteins, especially collagens (predominantly types I and III) are synthesized by the cardiac fibroblasts. Distortion of the extracellular matrix composition and protein architecture has profound implications on myocardial remodelling, plays a relevant role in the pathogenesis of many cardiac pathologies, and was shown to be the case in dilated cardiomyopathy.

The present work has sought to determine how the composition of extracellular matrix changes in a murine model of viral myocarditis by applying infra-red microspectroscopy. The primary purpose of this study was to demonstrate the compositional alterations in temporal relations with progression of that disease state.

The results of this study showed increased collagen correlations in mouse strains susceptible to progression to overt cardiomyopathy. This correlated with the evidently recognized myocardial fibrosis in chronic stages of cardiomyopathy

These data provide an indication of the importance of changes in collagen content in the adverse remodeling of the failing heart and, thus, raise the possibility of pharmacological

prevention of the degeneration of myocardial structure and function during the transition from acute phase of myocarditis to chronic cardiomyopathy.

Whether these findings are unique to the murine heart and thus not relevant to the human heart can only be answered by appropriate studies on human myocardium. However, previous studies have suggested that the human heart will show responses in the extracellular matrix similar to those in the mouse heart.

X. Acknowledgment

I would like to thank Lisa Miller (National Synchrotron Light Source) for the technical supervision and professional guidance, and Qi Wang for the technical assistance. Many thanks go also to Priv.-Doz. Dr. Karin Klingel (Universität Tübingen, Germany) for providing the mouse models and for the sample preparation. I would like to also express my gratitude to the NSLS for providing the facilities, which made this study possible.
Much appreciation goes to Prof. Dr. G. Baumann and Priv.-Doz. Dr. T. Dschietzig for the scientific supervision once the work thesis was initiated.

References

1. Virmani R, Burke AP, Farb A, Smialek J. Problems in forensic cardiac pathology. In: Schoen FJ, Gimbrone MA Jr, eds. Cardiovascular pathology: Clinicopathologic correlations and pathogenic mechanisms. Williams & Wilkins, Baltimore 1995:173-196.

2. Fabre A, Sheppard MN. Sudden adult death syndrome and other non ischaemic causes of sudden cardiac death: a UK experience. Heart 2005 [Epub ahead of print].

3. Feldman AM, McNamara D. Myocarditis. N Engl J Med 2000;343:1388-1398.

4. Kandolf R, Klingel K, Zell R, Selinka HC, et al. Molecular Pathogenesis of enterovirus-induced myocarditis: virus persistence and chronic inflammation. Intervirology 1993;35:140-151.

5. Cossart YE, Burgess JA, Nash PD. Fatal coxsackie B myocarditis in an adult. Med J Aust 1965;1:337-339.

6. Li Y, Bourlet T, Andreoletti L, et al. Enteroviral capsid protein VP1 is present in myocardial tissues from some patients with myocarditis or dilated cardiomyopathy. Circulation 2000; 101:231

7. Martino TA, Liu P, Sole MJ. Viral infection and the pathogenesis of dilated cardiomyopathy. Circ Res 1994;74:182-188.

8. Felker GM, Thompson RE, Hare JM, et al. Underlying causes and long-term survival in patients with initially unexplained cardiomyopathy. N Engl J Med 2000;342:1077-1084.

9. Maron BJ, Towbin JA, Thiene G, et al. Contemporary definitions and classification of the cardiomyopathies. Circulation 2006;113:1807-1816.

10. Figulla HR. Transformation of myocarditis and inflammatory cardiomayopathy to idiopathic dilated cardiomyopathy: facts and fiction. Med Microbiolo Immunol 2004;193:61-64.

11. Arbustini E, Gavazzi A, Dal Bello B, et al: Ten years experience with endomyocardial biopsy in myocarditis presenting with congestive heart failure: Frequency, pathologic characteristics, treatment, and follow-up. G Ital Cardiol 1997;27:209.

12. Brown RD, Ambler SK, Mitchell MD, et al. The cardiac fibroblast: therapeutic target in myocardial

13. Brown L. Cardiac extracellular matrix: a dynamic entity. Am J Physiol Heart Circ Physiol 2005;289:H973-H974.

14. Weber KT, Sun Y, Tyagi SC, et al. Collagen network of the myocardium: function, structural remodelling and regulatory mechanisms. J Mol Cell Cardiol 1994;26: 279–292.

15. Weber KT. From inflammation to fibrosis: a stiff stretch of highway. Hypertension 2004;43:716-19.

16. Spinale FG. Matrix metalloproteinases: regulation and dysregulation in the failing heart. Circ Res 2002;90:520–530

17. Baicu CF, Stroud JD, Livesay VA, et al. Changes in extracellular collagen matrix alter myocardial systolic performance. Am J Physiol Heart Circ Physiol 2003;284:H122–H132.

18. Boluyt MO, Bing OHL. Matrix gene expression and decompensated heart failure: the aged SHR model. Cardiovasc Res 2000;46:239–249.

19. Brilla CG, Weber KT. Reactive and reparative myocardial fibrosis in arterial hypertension in the rat. Cardiovasc Res 1992;26: 671–677.
20. Gunja-Smith Z, Morales AR, Romanelli R, et al. Remodeling of human myocardial collagen in idiopathic dilated cardiomyopathy: Role of metalloproteinases and pyridinoline cross-links. Am J Pathol 1996;148: 1639-1648

21. Perlini S, Palladini G, Ferrero I, et al. Sympathectomy or doxazosin, but not propranolol, blunt myocardial interstitial fibrosis in pressure overload hypertrophy. Hypertension 2005;46:1213–1218.

22. Klingel K, Hohenadl C, Canu A, et al. Ongoing enterovirus-induced myocarditis is associated with persistent heart muscle infection: Quantitative analysis of virus replication, tissue damage, and inflammation. Proc Natl Acad Sci USA 1992;89:314-318.

23. Liu KZ, Dixon IMC, Mantsch HH. Distribution of collagen deposition in cardiomyopathic hamster hearts determined by infrared microscopy. Cardiovasc Pathol 1999;8:41-47

24. Klingel K, Stephan S, Sauter M, et al. Pathogenesis of murine enterovirus myocarditis: Virus dissemination and immune cell targets.. J Virol 1996;70(12):8888-8895.

25. Griffiths PD, Hanningtn G, Booth GC. Coxsackie B virus infection and myocardial infarction: results from a prospective, epidemiologically controlled study. Lancet 1980;1:1387-1389.

26. Bowles, NE, Ni J, Kearney DL, et al. Detection of viruses in myocardial tissues by polymerase chain reaction: Evidence of adenovirus as a common cause of myocarditis in children and adults. J Am Coll Cardiol. 2003;42:466-472.

27. Satu Y, Yamanda T, matsumori A. Hepatitis C vrus and cardiomyopathy. In: Matsumori A, ed. Cardiomyopathy and heart failure: biomolecular, infectious, and immune mechanisms. Boston, Mass: Kluwer Academics Publishers; 2003:325-339.

28. Pankuweit S, Portig I, Lottspeich F, et al. Autoantibodies in sera of patients with myocarditis: characterization of the corresponding proteins by isoelectric focusing and N-terminal sequence analysis. J Mol Cell Cardiol 1997; 29:77-84.

29. Matsumori A, Matoba Y, Sasayama S. Dilated cardiomyopathy associated with hepatitis virus infection. Circulation 1995;92:2519-2525.

30. Herskowitz A, Wu TC, Willoughby SB, et al. Myocarditis and cardiotropic viral infection associated with severe left ventricular dysfunction in late-stage infection with human immunodeficiency virus. J Am Coll Cardiol 1994;24:1025-1032.

31. Hofman P, Drici MD, Gibelin P, et al. Prevalence of toxoplasma myocarditis in patients with the acquired immunodeficiency syndrome. Br Heart J 1993;70: 376-381

32. Pulerwitz TC, Cappola TP, Felker GM, et al. Mortality in primary and secondary myocarditis. Am Heart J. 2004; 147:746-750.

33. Barbaro G, Di Lorenzo G, Grisorio B, et al. For the Gruppo Italiano per lo Studio Cardiologico dei Pazienti Affetti da AIDS. Incidence of dilated cardiomyopathy and detection of HIV in myocardial cells of HIV-positive patients. N Engl J Med 1998;339:1093-1099.

34. Liu PP, Maso JW. Advances in understanding of myocarditis. Circulation 2005;104:1076-1082.

35. Liu PP, Schultheiss HP. Myocarditis. In: Libby P, Bonow RO, Mann DL, Zipes DP, eds. Braunwald's Heart disease: a textbook of cardiovascular medicine. 8th ed.. Saunders Elsevier 2008:1775-1792.

36. Bergelson JM, Cunningham JA, Druguett G, et al. Isolation of a common receptor for Coxsackie B viruses and adenoviruses 2 and 5. Science 1997;275:1320-1323.
37. Kawai C. From myocarditis to cardiomyopathy: Mechanisms of inflammation and cell death: Learning from the past for the future. Circulation. 1999;1091-1100.

38. Padalko E, Ohnishi T, Matsushita K, et al. Peroxynitrite inhibition of coxsackievirus infection by prevention of viral RNA entry. Proc Natl Acad Sci U S A. 2004;101:11731-11736.

39. Seko Y, Tsuchimochi H, Nakamura T, et al. Okumara Expression of major histocompatibility complex class I antigen in murine ventricular myocytes infected with Coxsackievirus B3. Circ Res 1990;67:360-367.

40. Kaya Z, Afanasyeva M, Wang Y, et al. Contributions of the innate immune system to autoimmune myocarditis: a role for complement. Nat Immunol 2001; 2:739-745.

41. Staudt A, Schaper F, Stangl V, et al. Immunohistological changes in dilated cardiomyopathy induced by immunoadsorption therapy and immunoglobulin substitution. Circulation. 2001;103:2681-2686

42. Kim KS, Tracey S, Tapprich W, et al. 5-Terminal deletions occur in Coxsackievirus B3 during replication in murine hearts and cardiac myocyte cultures and correlate with encapsidation of negative-strand viral RNA. J Virol 2005;79:7024-7041.

43. Wessely R, Henke A, Zell R, et al: Low level expression of a mutant coxsackieviral cDNA induces a myocytopathic effect in culture: an approach to the study of eteroviral persistence in cardiac myocytes. Circulation1998;98:450.

44. Sole MJ, Liu P: Viral myocarditis: A paradigm for understanding the pathogenesis and treatment of dilated cardiomopathy. J Am Coll Cardiol 1993;22:99A

45. Baughman KL, Wynne J. Myocarditis. In: Zipes DP, Libby P, Bonow PO, Braunwald E, eds. Braunwald's heart disease. 7th ed. Philadelphia, USA Elsevier Saunders. 2005:1697-1717.

46. Bendall JK, C Heymes, P Ratajczak P, et al. Extracellular matrix and cardiac remodeling. Arch Mal Coeur Vaiss 2002; 95:1226-1229

47. Tomita H, Egashira K, Ohara Y, et al. Early induction of transforming growth factor-beta via angiotensin II type 1 receptors contributes to cardiac fibrosis induced by long-term blockade of nitric oxide synthesis in rats. Hypertension 1998;32:273-9.

48. Nakajima H, Nakajima HO, Salcher O, et al. Atrial but not ventricular fibrosis in mice expressing a mutant transforming growth factor-beta(1) transgene in the heart. Circ Res 2000;86:571-579

49. Rosenkranz S, Flesch M, Amann K, et al. Alterations of beta-adrenergic signaling and cardiac hypertrophy in transgenic mice overexpressing TGF-beta(1). Am J Physiol Heart Circ Physiol. 2002;283:H1253-62.

50. Schultz Jel J, Witt SA, Glascock BJ, et al. TGF-beta1 mediates the hypertrophic cardiomyocyte growth induced by angiotensin II. J Clin Invest 2002;109:787-796.

51. Klein G, Schaefer A, Hilfiker-Kleiner D. et al. Increased collagen deposition and diastolic dysfunction but preserved myocardial hypertrophy following pressure overload in mice lacking PKC. Circ Res 2005;96(7):748-755.

52. Verheule S, Sato T, Everett T 4th, et al. Increased vulnerability to atrial fibrillation in transgenic mice with selective atrial fibrosis caused by overexpression of TGF-α. Circ Res 2004; 94:1458-65.

53. Walker GA, Masters KS, Shah DN, et al. Valvular myofibroblast activation by transforming growth factor-beta: implications for pathological extracellular matrix remodeling in heart valve disease. Circ Res 2004;95:253-60.

54. Marijianowski MM, Teeling P, Mann J, et al. Dilated cardiomyopathy is associated with an increase in the type I/type III collagen ratio: a quantitative assessment. J Am Coll Cardiol 1995; 25:1263-72.

55. Sanderson JE, LaiK B, ShumI O, et al. Transforming growth factor-beta (1) expression in dilated cardiomyopathy. Heart 2001; 86:701-8

56. Holweg CT, Baan CC, Niesters HG, et al. Vantrimpont TGF-beta1 gene polymorphisms in patients with end-stage heart failure. J Heart Lung Transplant 2001;20: 979-84.

57. Yamada Y, Miyauchi A, Takagi Y, et al. Association of a polymorphism of the transforming growth factor-beta1 gene with genetic susceptibility to osteoporosis in postmenopausal Japanese women. J Bone Miner Res 1998;13:1569-76

58. Dec GW. Introduction to clinical myocarditis. In: Cooper LT, ed. Myocarditis: From Bench to Bedside. Totowa, NJ: Humana Press; 2003;257-281.

59. Magnani JW, Dec W. Myocarditis: Current trends in diagnosis and treatment. Circulation. 2006;113:876-980.

60. Mason JW, O'Connell JB, Herzkowitz A, et al for the Myocarditis Treatment Trial Investigators. A clinical trial of immunosuppressive therapy for myocarditis. N Engl J Med 1995;333:269-275.

61. Dec GW, Palacios IF, Fallon JT, et al. Active myocarditis in the spectrum of acute dilated cardiomyopathies: clinical features, histologic correlates, and clinical outcome. N Engl J Med 1985;312:885-890.

62. Liebeman EB, Hutchins GM, Herskowsk A, et al. Clinicopathological description of myocarditis. J Am Coll Cardiol 1991;18:1617-1626.

63. McCarthy RI III, Boehmer JP, Hruban RH, et al. Long-term outcome of fulminant myocarditis as compared with acute (nonfulminant) myocarditis. N Engl J Med 2000;342:692-695.

64. Angelini A, Calzolari V, Calabrese F, et al. Myocarditis mimicking acute myocardial infarction: role of endomyocardial biopsy in the differential diagnosis. Heart. 2000;84:245-250.

65. Sarda L, Colin P, Boccara F, et al. Myocarditis in patients with clinical presentation of myocardial infarction and normal coronary angiograms. J Am Coll Cardiol. 2001;37:786-792.

66. Smith SC, Ladenson JH, Mason JW, et al. Elevations of cardiac troponin I associated with myocarditis: experimental and clinical correlates. Circulation 1997;95:163-168.

67. Dec GW, Waldman H, Southern J, et al. Viral myocarditis mimicking acute myocardial infarction. J Am Coll Cardiol 1992;20: 85-89.

68. Mason JW. Techniques for right and left and right ventricular endomyocardial biopsy. Am J Cardiolo 1978;41:887-892

69. Anderson JL, Marshall HW. The femoral venous approach to endomyocardial biopsy: comparison with internal jugular and transarterial approaches, Am J Cardiol 1984;53:833-837.

70. Rios B, M.R. Nihill MR, Mullins CE. Left ventricular endomyocardial biopsy in children with the transseptal long sheath technique, Cathet Cardiovasc Diagn. 1984;10:417-423.

71. Mahrholdt H, Goedecke C, Wagner A, et al. Cardiovascular magnetic resonance assessment of human myocarditis: a comparison to histology and molecular pathology. Circulation 2004;109:1250-1258.

72. Cooper LT, Baughman K, Feldman AM, et al. The role of endomyocardial biopsy in the management of cardiovascular disease: a scientific statement from the American Heart Association, the American College of Cardiology, and the European Society of Cardiology. J Am Coll Cardiol 2007;50:1914-31.

73. Wynne J, Braunwald E. The cardiomyopathies. In: Zipes DP, Libby P, Bonow RO, Braunwald E, eds. Braunwald's heart disease. 7th ed. Elsevier Saunders. 2005:1659-1696.

74. McNamara DM, Holubkov R, Starling RC, et al: Controlled trial of intravenous immune globulins in recent-onset dilated cardiomyopathy. Circulation 2001;103:2254.

75. Mills RM, Lauer MS. Endomyocardial biopsy: A procedure in search for an indication. Am Heart J; 2004;147:759-760.

76. Chow LH, Radio SJ, Sears TD, et al. Insensitivity of right ventricular endomyocardial Biopsy in the diagnosis of myocarditis. J Am Coll Cardiol. 1989;14:915-920.

77. Hauck AJ, Kearney DL, Edwards WD. Evalution of postmortem endomyocardial biops specimens from 38 patients with lymphocytic myocarditis:Implications for the roll of sampling error. Mayo Clin Proc 1989;64:1235-1245.

78. Baughman KL. Diagnosis of myocarditis: Death of Dallas criteria. Circulation 2006;113:593-595.

79. Martin AB, webber S, Fricker FJ, et al. Jaffe Acute myocarditis; rapid diagnosis by PCR in children. Circulation 1994;90:330-339.

80. Cassling RS, Linder J, Sears TD, et al. Quantitative evaluation of inflammation in biopsy specimens from idiopathically failing or irritable hearts: experience in 80 pediatric and adult patients. Am Heart J 1985;110:713-720.

81. Kuhl U, Seeberg B, Schultheiss HP, et al. Immunohistological characterization of infiltrating lymphocytes in biopsies of patients with clinically suspected dilated cardiomyopathy. Eur Heart J 1994; 15(suppl C):62-67.

82. Wojnicz R, Nowalany-Kozielska E, et al. Immunohistological diagnosis of myocarditis: potential role of sarcolemmal induction of the MHC and ICAM-1 in the detection of autoimmune mediated myocyte injury. Eur Heart J. 1998;19:1564-1572

83. Wojnicz R, Nowalany-Kozielska E, et al. Randomized, placebo-controlled study for immunosuppressive treatment of inflammatory dilated cardiomyopathy: two-year follow-up results. Circulation 2001;104:39-45.

84. Parrillo JE, Cunnion RE, Epstein SE, et al. A prospective, randomized, controlled trial of prednisone for dilated cardiomyopathy. N Engl J Med 1989;321:1061

85. Huber S. Cellular autoimmunity in myocarditis. Heart Fail Clin 2005; 1:321-331.

86. Dec GW, Palacios I, Yasuda T, et al. Antimyosin antibody cardiac imaging: its role in the diagnosis of myocarditis. J Am Coll Cardiol. 1990;16:97-104.

87. Margari ZJ, Anastasiou-Nana MI, Terrovitis J, et al. Indium-111 monoclonal antimyosin cardiac scintigraphy in suspected active myocarditis: evolution and diagnostic impact. Int J Cardiol 2003; 90:239-245.

88. O'Connel JB, Henkin RF, Robinson JA, et al. Gallium-67 imaging in patients with dilated cardiomyopathy and biopsy-proven myocarditis. Circulation 1984;70:58-62.

89. Laissy JP, Messin B, Varenne O, et al. MRI of acute myocarditis: a comprehensive approach based on various imaging sequences. Chest 2002;122:1638-1648.

90. McManus BM, Chow LH, Wilson JE, et al. Direct myocardial injury by enterovirus: a central role in the evolution of murine myocarditis. Clin Immunol Immunopathol 1993;68:159-169

91. Kandolf R, Canu H, Hofschneider PH. Coxsackie B virus can replicate in cultured human foetal heart cells and is inhibited by interferon. J Mol Cell Cardiol 1985;17:167-181.

92. Yoneda S, Senda K, Hayashi K. Experimental study of virus myocarditis in culture. Jpn Circ J 1979;43:1048-1054.

93. Mall G, klingel K, Albrecht M, et al. Natural history of Coxsackievirus B3-induced myocarditis in ACA/Sn mice: Viral persistence demonstrated by quantitative in situ hybridization histobiochemistry. Eur Heart J 1991;12 Suppl D:121-123.

94. Chow LH, Bisel KW, McManus BM. Enteroviral infection of mice with severe combined immunodeficiency: Evidence for direct viral pathogenesis of myocardial injury. Lab Invest 1992;66:24-31.

95. Heim A, Stille-siegener M, kandolff R, et al. Enterovirus-induced mycarditis: hemodynamic deterioration with immunosuppressive therapy and successful application of interferon-alpha. Clin Cardiol 1994;17:563-565.

96. Wilson FM, Miranda QR, Chason JL, et al. Residual pathologic changes following murine Coxsackie A and b myocarditis. Am J Pathol 1969;55:253-265.

97. Miller LM, Dumas P. Chemical imaging of biological tissue with synchrotron infrared light. Biochimica et Biophysica Acta (BBA) - Biomembranes, 2006;1758(7):846-857.

98. Humecki H. Practical Applications of Infrared Microspectroscopy. Marcel Dekker Inc., New York. 1995.

99. Lewis EN, Treado PJ, , Reeder RC, et al. Fourier-transform spectroscopic imaging using an infrared focal-plane array detector. Anal. Chem 1995;67:3377-3381

100. Huffman WS, Bhargava R, Levin IW. Generalized implementation of rapid-scan Fourier transform infrared spectroscopic imaging. Appl. Spectrosc 2002;56:965-969.

101. Messerschmidt RG. In: H. Humecki H., ed. Practical Guide to Infrared Microspectroscopy. Marcel Dekker, Inc., New York 1995:3-40.

102. Kandolf R, Hofschneider PH. Molecular cloning of the genome of a cardiotropic Coxsackie B3 virus: full-length reverse-transcribed recombinant cDNA generates infectious virus in mammalian cells. Proc. Natl. Acad. Sci. U.S.A. 1985;82(14):4818-4822

103. Gough KM, Zelinski D, Wiens R, et al. Fourier transform infrared evaluation of microscopic scarring in the cardiomyopathic heaert: effect of chronic AT1 suppression. Anal. Biochem 2003;316(2):232-242.

104. Strobeck JE, Factor SM, Bhan A, et al. Hereditary and acquired cardiomyopathies in experimental animals: mechanical, biochemical, and structural features. Ann. N.Y. Acad. Sci. 1979;317:59-88.

105. Davison G, Hall CS, Miller JG, et al. Cellular mechanisms of captopril-induced matrix remodelling in Syrian hamster cardiomyopathy. Circulation 1994;90(3):1334-1342.

106. Liu K, Jackson M, Sowa MG, et al. Modification of the extracellular matrix following myocardial infarction monitored by FTIR spectroscopy. Biochim. Biophys. Acta 1996;1315(2):73-77.

107. Stuart B. In: Ando DJ, eds. Biological Applications of Infrared Spectroscopy, John Wiley and Sons, Inc., Chichester 1997:113-153.

108. Camacho NP, West P, Torzilli PA, Mendelsohn R. FTIR microscopic imaging of collagen and proteoglycans in bovine cartilage. Biopolymers 2001;62(1):1-8.

109. Klingel K, Schnorr JJ, Sauter M, et al. Beta2-microglobulin-associated regulation of interferon-gamma and virus-specific immunoglobulin G confer resistance against the development of chronic coxsackievirus myocarditis Am. J. Pathol. 2003;162(5):1709-1720.

110. Massie BM. 2008. Heart failure: Pathophysiology and diagnosis. In: Goldmann l, Ausiello D, eds. Cecil Textbook of Medicine, 23th ed. Philadelphia, USA. 2008:341-345.

111. Kannel WB. Epidemiology of heart failure in the United States. In: Poole-Wilson PA, Colucci WS, Massie BM, Catterjee K, Coats AJS, eds. Heart failure. NY: Churchill Livingston 1997:279-288

112. Preston LC, Lipscomb S, Robinson B, et al. Functional effects of the DCM mutant Gly159Asp Troponin C in skinned muscle fibers. Pflugers Arch-Eur J Physiol 2007;453:771-776

113. Ellis CR, Di salvo T. Myocarditis: basic and clinical aspects. Cardiol in Rev 2007;15:170-177

114. Moloney ED, Egan JJ, Kelly P, et al. Transplantation for myocarditis: a controversy revisited. J Heart Lung Transplant 2005;24:1103-1110

115. Eckart RE, Scoville SL, Campbell CL, et al. Sudden death in young adults: a 25-year review of autopsies in military recruits. Ann Inten Med 2004;141:829-834

116. Peters N, Poole-Wilson P. Myocarditis: continuing clinical and pathologic confusion. Am Heart J 1991;121:942-946

117. Weinstein C, Fenoglio J. Myocarditis. Hum Pathol 1987;18:613-618

118. Aretz H. Myocarditis: the Dallas criteria. Hum Pathol 1987;18:619-624

119. Maisch B, Ristie A Portig I, pankoweit S. Human viral cardiomyopathy. Front Biosci 2003;8:39-67

120. Blankenhorn MA, Gall EA. Myocarditis and myocardosis; a clinopathologic appraisal. Circulation 1956;13:217-223

121. Fuse K, Kodama M, Okura Y, et al. Predictors of disease course in patients with acuta myocarditis. Circulation 2000;102:2829:2835

122. Nishii M, Inomata T; Takehanan H, et al. Serum levels of interleukin-10 on admission as a prognostic predictor of human fulminant myocarditis. J Am Coll Cardiol 2004;44:1292-1297

123. Sheppard R, Bedi M, Kubota T, et al. Myocardial expression of fas and recovery of left ventricular function in patients with recent-onset cardiomyopathy. J Am Coll cardiol 2005;46:1036-1042

124. Lauer B, Schannwell M, Kuhl U, et al. Antimyosin autoantibodies are associated with deterioration of systolic and diastolic left ventricular function in patients with chronic myocarditis. J Am Coll cardiol 2000;35:11-18

125. Kuhl U, Pauschinger M, Seeberg B, et al. Viral persistence in the myocardium is associated with progressive cardiac dysfunction. Circulation 2005;112:1965-1970

126. Leipner C, Grun K, Borchers M, et al. The outcome of coxsackievirus B3-(CVB-3) induced myocarditis is influenced by the cellular immune status. Herz 2000;25:245-248

127. Bashey RI, Martinez-Hemandez A, Jimenez SA. Isolation, characterization, and localization of cardiac collagen type IV. Association with other extracellular matrix components. Circ Res 1992;70:1006-1017.

128. Mann DL. Pathophysiology of heart failure. In: Libby P, Bonow RO, Mann DL, Zipes DP, eds. Braunwald's Heart disease: a textbook of cardiovascular medicine. 8th ed.. Saunders Elsevier 2008:541-560.

129. Opie LH. In: Heart physiology: From cell to circulation, ed., Lippincott W & W. 4th ed. 2004:331.

130. Woodiwiss AJ, et al. Reduction in myocardial collagen cross-linking parallels left ventricular dilatation in rat models of systolic chamber dysfunction. Circulation 2001;103:155-160.

131. Deschamps AM, Spinale FG: Matrix modulation and heart failure: new concepts questions old beliefs. Curr Poin Cardiol 2005;20:211.

132. Mann DL. Left ventricular size and shape: determinants of mechanical signal transduction pathways. Heart Fail Rev 2005;10:95.

133. Maekawa Y, Ouzounian M, Opavsky A, et al. Connecting the missing link between dilated cardiomyopathy and viral myocarditis: Virus, Cytoskeleton, and innate immunity. Circulation 2007;115:5-8.

134. Marino T, Petric M, Weingart H, et al. The coxsackie-adenovirus receptor (CAR) is used by reference strains and clinical isolates representing all 6 stereotypes of coxsackievirus group B, and by swine vescicular disease virus. J virol 2000;271:99-108.

135. Badorff C, Lee GH, Lamphear ME, et al. Enteroviral protease 2A cleaves dystrophin: evidence of cytoskeletal disruption in an acquired cardiomyopathy. Nat Med 1999;5:320-326.

136. Xiong D, Yajima T, Lim B-K, Stenbit A, et al. Inducible cardiac restricted expression of enteroviral protease 2A is sufficient to induce dilated cardiomyopathy. Circulation 2007;115.94-102.

137. Liu KZ, Dixon IMC, Mantsch HH. Distribution of collagen deposition in cardiomyopathic hamster hearts determined by infrared microscopy. Cardiovasc Pathol 1999;8:41-47.

138. Grist NR, Reid D. Organisms in myocarditis/endocarditis viruses. J Infect 1997;34:155.

Mein Lebenslauf wird aus Datenschutzgründen in der elektronischen Version meiner Arbeit nicht veröffentlicht.

Wasiem G.E. Sanad

Erklärung

Ich, Wasiem G.E. Sanad, erkläre, dass ich die vorgelegte Dissertationsschrift mit dem Thema

Ultrastructural and Compositional Changes in Heart Muscle Cells in Mouse Model of Viral Myocarditis as Imaged by Infra-red Spectromicroscopy

Selbst verfasst und keine anderen als die angegebenen Quellen und Hilfsmittel benutzt, ohne die unzulässige Hilfe Dritter verfasst und auch in Teilen keine Kopien anderer Arbeiten dargestellt habe.

01.03.2008 Wasiem Sanad